

Determining the Zero-Field Cooling/ Field Cooling Blocking Temperature from AC-Susceptibility data for Single-Molecule Magnets

Yolimar Gil,^a María Mar Quesada-Moreno,^b María A. Palacios,^c Silvia Gómez-Coca,^d Enrique Colacio,^c Eliseo Ruiz,^d Daniel Aravena,^e

^a Facultad de Ciencias Químicas y Farmacéuticas, Universidad de Chile,
Casilla 233, Santiago, Chile

^b Departamento de Química Física y Analítica, Universidad de Jaén, Campus Las Lagunillas,
23071, Jaén, Spain

^c Departamento de Química Inorgánica, Facultad de Ciencias,
Universidad de Granada, 18071Granada, Spain

^d Departament de Química Inorgànica i Orgànica and Institut de Recerca de Química
Teòrica i Computacional, Universitat de Barcelona, Diagonal 645, 08028 Barcelona,
Spain

^e Departamento de Química de los Materiales, Facultad de Química y Biología,
Universidad de Santiago de Chile, Casilla 40, Correo 33, Santiago, Chile

Table of Contents

1. Experimental Section
 - 1.1. Synthetic procedures
 - 1.2. Thermogravimetric Analysis
 - 1.3. Physical measurements details
 - 1.4. Single-Crystal Structure Determinations
2. Magnetic Studies
 - 2.1. Susceptibility and magnetisation
 - 2.2. Zero Field Cool / Field Cool
 - 2.3. In-phase and out-of-phase magnetic susceptibility
 - 2.4. Magnetisation decay
3. Ab initio calculations
4. Theoretical Model
5. Model Assessment
6. References

1. Experimental Section

1.1. Synthetic procedures

All reactions were conducted in aerobic conditions and the analytical reagents were purchased from commercial sources and used without further purification. The di(1-adamantyl)benzylphosphine was purchased from Sigma-Aldrich. The anhydrous compounds (the DyBr₃ salt and the tetrahydrofuran solvent) were always kept under inert atmosphere conditions.

Oxidation of the di(1-adamantyl)benzylphosphine

In a round-bottom flask, the di(1-adamantyl)benzylphosphine (0.5 g, 1.274 mmol) was dissolved in the minimum amount of methylene chloride and reacted with an excess of 30 % hydrogen peroxide in water (10 mL/g of di(1-adamantyl)benzylphosphine) and allowed to stir under ambient conditions for 12 hours, during which time the solution changed from clear to light yellow in colour. Upon completion, the reaction mixture was washed three times with water, then three times with brine solution, dried with sodium sulphate and filtered. Finally, the solvent was removed under reduced pressure. Yield: 85%. IR (cm⁻¹): IR (cm⁻¹): 3000-2800, v(C-H, alkyl and aromatic); 1601, v(C-C, aromatic); 1500-1300, bending(C-H, alkyl and aromatic); 1200-1100, v(P=O); 698, ω(C-H, aromatic) and v(P-C); 590, (in-plane benzene ring def.).

¹H NMR (360 MHz, CDCl₃): δ 7.47-7.18 (m, 5H), 3.15 (d, 2H), 2.17-1.70 (m, 30H).

³¹P NMR (203 MHz, CDCl₃): δ 48.45 (s).

Synthesis of [Dy(OPAd₂Bz)₂(H₂O)₄Br]Br₂·4THF (1)

A solution of the anhydrous DyBr₃ solid (48.27 mg, 0.12 mmol) in THF (7 mL) was heated at 80 °C in aerobic conditions until DyBr₃ was dissolved. The colour of the solution changed from clear to yellow. Additional THF was added when necessary while heating. After that, the ligand di(1-adamantyl)benzylphosphine oxide (100 mg, 0.24 mmol) was added, and THF was also added until reaching a final volume of 10 ml. The resulting mixture was sealed in a 15 ml teflon-lined stainless container and kept at 100 °C for three days. The solution obtained was transferred to a beaker and left to stand for 10 minutes, so that the little precipitate obtained remains at the bottom. Then, the solution is taken from the upper part. Crystallisation from slow evaporation produces air/humidity stable and large colourless prismatic single-crystals with a yield of 79%. Anal. Calc. for C₇₀H₁₁₄Br₃DyO₁₀P₂ (1581.82): C, 53.22; H, 7.27; N, 0; Found C, 52.89; H, 6.92; N, 0. IR (cm⁻¹): 3000-2800, v(C-H, alkyl and aromatic); 1601, v(C-C, aromatic); 1500-1300, bending(C-H, alkyl and aromatic); 1100-1000, v(P=O) and v(C-O, THF); 698, ω(C-H, aromatic) and v(P-C); 590, in-plane benzene ring def. The amount of THF molecules was determined by TG analysis (see next section).

1.2. Thermogravimetric Analysis (TGA)

TGA measurements of **1** were performed on a METTLER-TOLEDO instrument, mod. TGA/DSC1.

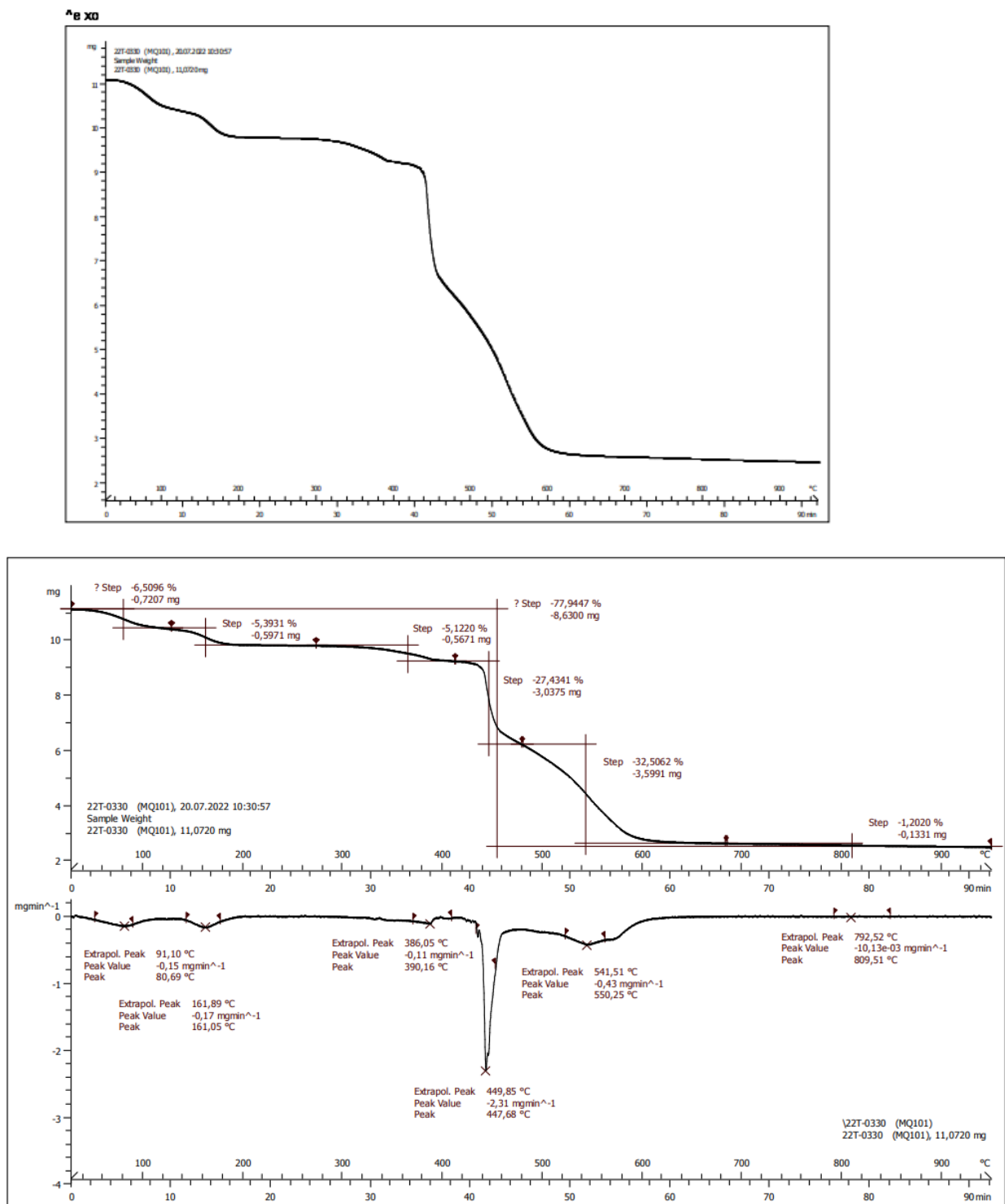


Figure S1. Thermogravimetric analysis (TGA) of **1** at a heating rate of 10 °C/min from 25 to 100 °C under nitrogen purging.

1.3. Physical measurements details

Elemental analysis was performed on a THERMO SCIENTIFIC Model Flash 2000 and ^1H NMR and ^{31}P { ^1H } RMN spectra on a 400 Hz “VARIAN DIRECT DRIVE” spectrometer at the “Centro de Instrumentación Científica” (University of Granada). IR spectra were recorded on a Bruker Tensor 27 spectrophotometer by using ATR detection. The X-ray powder diffraction (XRPD) spectrum was registered on a Bruker D8 DISCOVER using CuK α ($\lambda = 1.5406 \text{ \AA}$) radiation and DECTRIS PILATUS3R 100K-A detector, from 5 to 70° (2θ) at a scanning rate of $0.02^\circ 2\theta/\text{min}$.

1.4. Single-Crystal Structure Determinations

Suitable crystals of **1** were mounted on a glass fibre and used for data collection. X-ray diffraction data were collected at 100 K using a Bruker D8 Venture diffractometer (MoK α radiation, $\lambda = 0.71073 \text{ \AA}$) outfitted with a PHOTON III detector. Unit-cell parameters were determined and refined on all observed reflections using APEX2 software.^{1a} Correction for Lorentz polarization and absorption were applied by SAINT^{1b} and SADABS² programs, respectively.

The structures were solved using SHELXT³ by the intrinsic phasing method and refined by the full-matrix least-squares method on F2 using SHELXL-2014⁴ and the OLEX2 program.⁵ All non-hydrogen atoms were anisotropically refined. Hydrogen atom positions were calculated and isotropically refined as riding models to their parent atoms. One of the THF solvent molecules in structure **1** is disordered (oxygen 5 and carbon atoms C33, C34 and C35), and the disorder model was satisfactory. This model was not satisfactory when C32 was included in it; for this reason, C32 has not been split. The unit cell contains solvent-accessible VOIDS of 182 \AA^3 . This is due to the evaporation of a THF molecule, and fortunately, it kept the crystal intact.

A summary of selected data collection and refinement parameters can be found in Table S2 and CCDC 2372498.

Table S1. Continuous Shape Measures for **1**.

Comple x	JETPY-7	JPBPY-7	CTPR-7	COC-7	PBPY-7	HPY-7	HP-7
1	23.027	2.731	6.488	8.128	0.948	25.781	33.952

JETPY-7: Johnson elongated triangular pyramid J7 (C_{3v}); JPBPY-7: Johnson pentagonal bipyramid J13 (D_{5h}); CTPR-7: Capped trigonal prism (C_{2v}); COC-7: Capped octahedron (C_{3v}); PBPY-7: Pentagonal bipyramid (D_{5h}); HPY-7: Hexagonal pyramid (C_{6v}); HP-7: Heptagon (D_{7h}).

Table S2. Crystallographic data for complex **1**.

Compound	1
Formula	C ₇₀ H ₁₁₄ Br ₃ DyO ₁₀ P ₂
M_r	1579.78
Crystal System	tetragonal
Space Group	I4 ₁
a (Å)	24.7229(5)
b (Å)	24.7229(5)
c (Å)	12.1090(3)
α (°)	90
β (°)	90
γ (°)	90
V (Å³)	7401.3(4)
Z	4
D_c (g cm⁻³)	1.418
μ(MoK_α) (mm⁻¹)	2.725
T (K)	100
Observed reflections^a	11235 (10398)
R_{int}^a	0.0387 (0.0369)
Parameters	419
GOF	1.057
R₁^{b,a}	0.0341 (0.0300)
wR₂^{c,a}	0.0849 (0.0806)

^a Values in parentheses for reflections with I > 2σ(I)
^b R1 = $\sum ||F_o| - |F_c|| / \sum |F_o|$
^c wR2 = $\{\sum [w(F_o^2 - F_c^2)^2] / \sum [w(F_o^2)^2]\}^{1/2}$

Table S3. Selected bond distances (Å) and angles (°) for complex **1**.

Selected bond distances (Å)	
Dy – O1	2.210(3)
Dy – Br1	2.8860(6)
Dy – O2	2.349(3)
Dy – O3	2.380(3)
O1 – P1	1.516(3)
Selected bond angles (°)	
O1 – Dy – O1	176.73(16)
Br1 – Dy – O2	74.24(9)
O2 – Dy – O3	71.88(13)
O3 – Dy – O3	68.12(17)
O1 – Dy – Br1	91.64(8)
O1 – Dy – O2	88.13(11)
O1 – Dy – O3	90.70(11)
P1 – O1 – Dy	173.67(19)

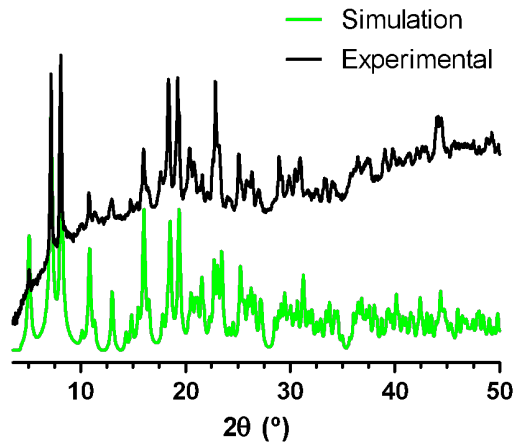


Figure S2. X-ray powder diffractogram for **1** (black) and the calculated from the X-ray crystal structure (green).

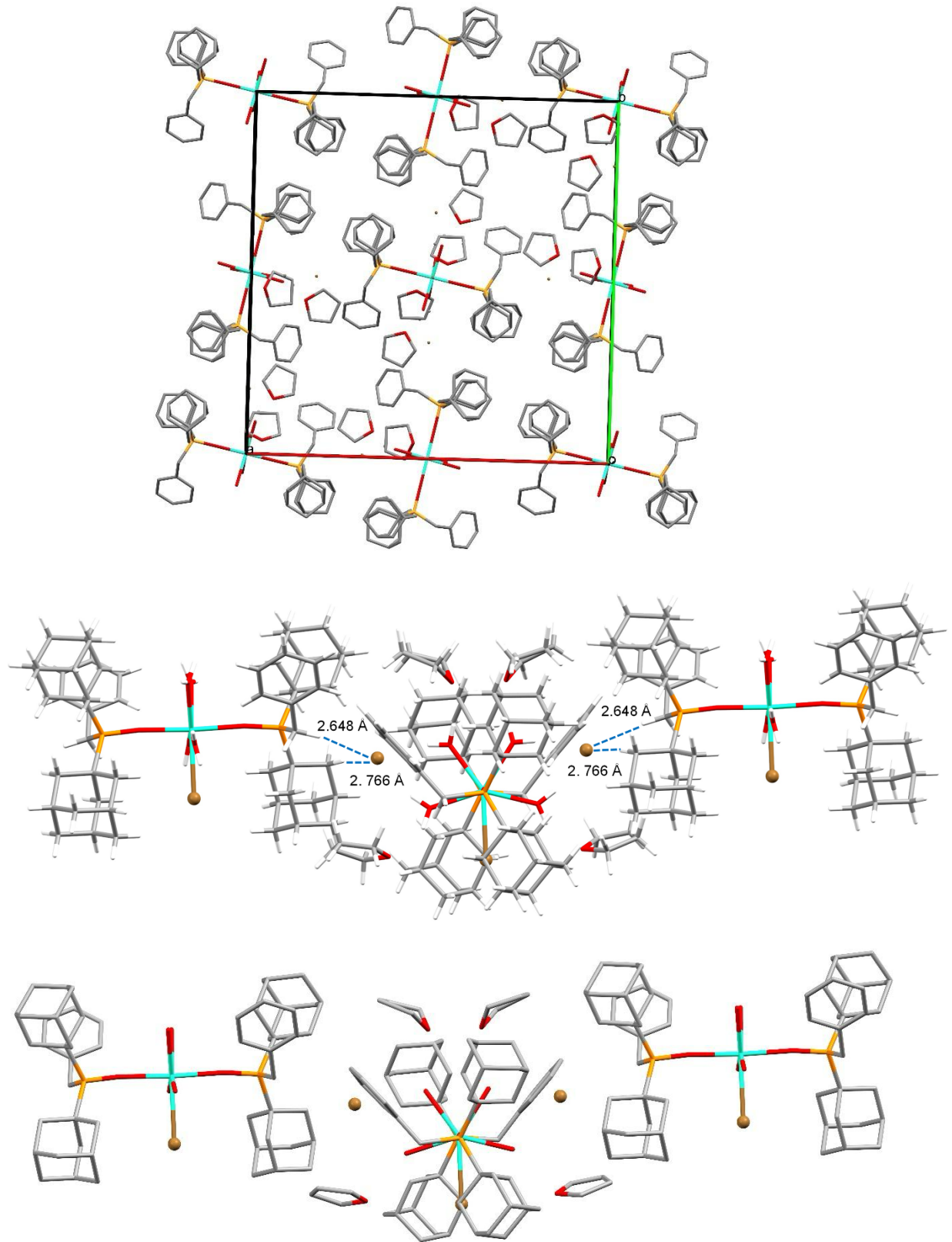


Figure S3. (top) A view of the crystal packing of **1** along the c axis. (middle) van der Waals interactions between adjacent units. Bromide atoms are displayed as brown balls. (bottom) The same view as “middle”, with the hydrogen atoms omitted for clarity.

2. Magnetic Studies

The DC magnetic measurements were performed on a polycrystalline sample of **1** using a Quantum Design SQUID MPMS XL-7 device. The temperature dependence of magnetic susceptibility has been measured in the 2-300 K range. The magnetic field dependence of magnetization has been measured under different applied static fields (0-7 T) in the temperature range 2-7 K. The magnetic susceptibility values were corrected for the diamagnetism of the molecular constituents, using the Pascal constants, and the sample holder.

The Zero Field Cool / Field Cool (ZFC/FC) experiment was performed under different conditions by varying the applied field as well as the measurement rate. The sample was initially cooled in absence of an external direct magnetic field. After reaching 2 K, a small magnetic field (50 or 500 Oe) was applied, and the magnetic moment was measured in sweep mode while increasing the temperature to 12 K at a specific rate (from 0.01 to 5 K/min). Then, the sample was cooled again to 2K while applying the field employed for the measurement and the magnetic moment was measured again in the same way. Between measurements at different rates the sample was heated in the absence of a magnetic field. The blocking temperatures for different heating rates and applied DC fields are collected in Table S4.

The in-phase and out-of-phase ac magnetic susceptibility measurements were carried out on a polycrystalline sample of **1**. To allow the study for a larger range of frequencies two equipment were employed. A PPMS-9 physical measurement equipment was employed for 100-10000 Hz frequency range, with an oscillating field $H_{ac} = 10$ Oe and using temperatures in the 2-56 K range. And a SQUID MPMS XL device was employed in the 1-1500 Hz frequency range with an oscillating field of 4 Oe between 15 and 27 K. The Cole-Cole plots were represented between 15 and 27 K and the relaxation time obtained by fitting the curves to the generalized Debye model. Obtained values are summarized in Table S5.

Isothermal magnetisation decay data was collected in the 2-8 K range. Firstly, at the selected temperature the sample was magnetized under an applied magnetic field of 5 T for 5 minutes. The field was set to zero on “No Overshoot” mode and the magnetisation measured for 2500 s. The magnetisation, however, equilibrated to a negative value, indicating a remanent field in the superconducting magnet. The data was fitted using a stretched exponential function, which is commonly employed in the obtention of relaxation times from magnetisation decay.^{6,7} The data was fit by employing Eq. S1 where M_{eq} is the negative equilibrium magnetisation values obtained at each experiment, M_0 is the first datapoint measured, t is the time in seconds since the first measurement, τ is the relaxation time and β is a stretching parameter ($0 < \beta \leq 1$). Obtained values are summarized in Table S6.

$$M = M_{eq} + (M_0 - M_{eq})e^{-(\frac{t}{\tau})^\beta} \quad (\text{S1})$$

The DC hysteresis measurements were collected in the 3- 20 K and at a sweep rate of 20mT/s on a Quantum Design instrument, model PPMS-9 (VSM option).

2.1 Susceptibility and magnetisation

The DC magnetic properties of **1** were studied in the 2-300 K temperature range under an applied magnetic field of 0.5 T plotted as $\chi_M T$ vs. T in Fig. S4.a) (χ_M is the molar magnetic susceptibility), with the isothermal magnetisation (M vs. H) shown in Fig. S4.a) (inset).

At 300 K, the $\chi_M T$ value of $14.65 \text{ cm}^3 \text{ K mol}^{-1}$ agrees with that expected for an isolated Dy^{III} ion ($4f^9$, $J = 15/2$, $S = 5/2$, $L = 5$, $g = 4/3$, ${}^6\text{H}_{15/2}$) in the free ion approximation ($14.18 \text{ cm}^3 \text{ K mol}^{-1}$). Upon cooling, the $\chi_M T$ value gradually decreases to $11.76 \text{ cm}^3 \text{ K mol}^{-1}$ at 7 K before rapidly decreasing to the value of $6.21 \text{ cm}^3 \text{ K mol}^{-1}$ at 2 K, which is characteristic of magnetically anisotropic lanthanide systems.

The gradual decrease is consistent with the thermal depopulation of the higher-energy $\pm m_J$ sublevels, which come from the splitting of the spin-orbit ground term ${}^6\text{H}_{15/2}$ by the crystal field effects. This indicates the existence of a large magnetic anisotropy with well-separated low-lying energy levels.

The field dependence of the magnetisation at 2 K (Fig. S4.b)) shows a sinusoidal behaviour at a low field with a saturation value of $6.00 N \mu_B$ at 7 T, which is expected for this kind of SMM. This low saturation value confirms the axial nature ($\pm 15/2$) of the well-isolated ground state.

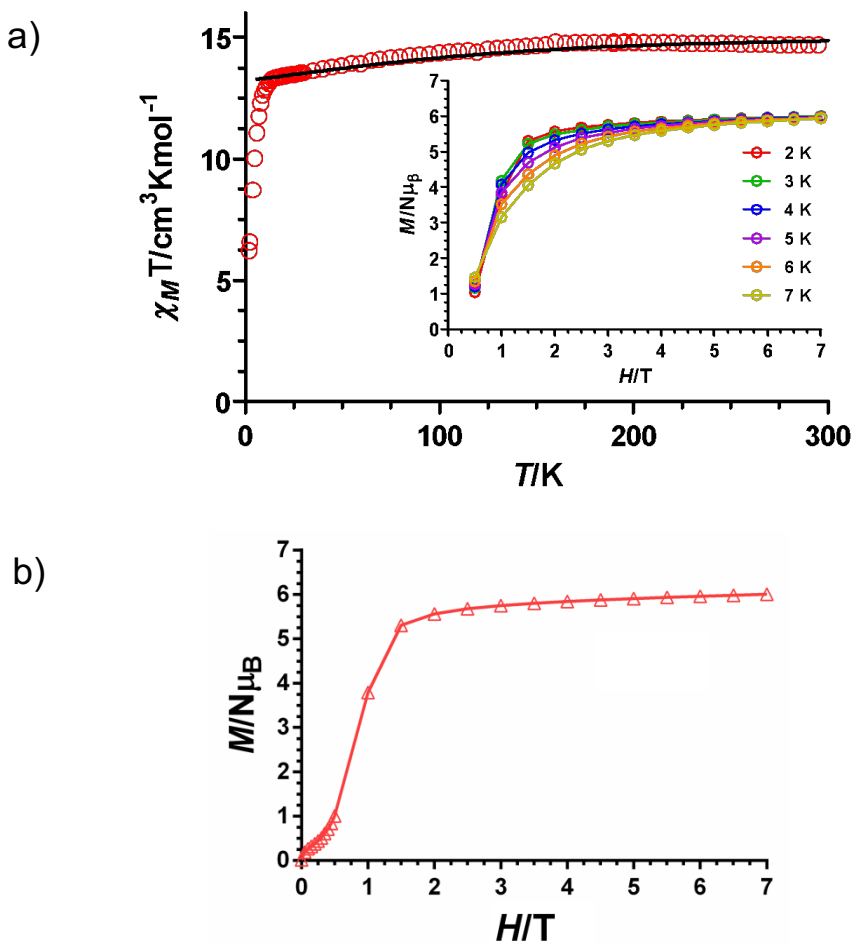


Figure S4. a) Temperature dependence of $\chi_M T$ for **1** (red circles) and that obtained using *ab initio* calculations (solid line, scaled by 1.07). Inset: Magnetisation vs. Field plot at the indicated temperatures; b) Magnetisation vs. Field plot at 2 K.

2.2 Zero Field Cool / Field Cool

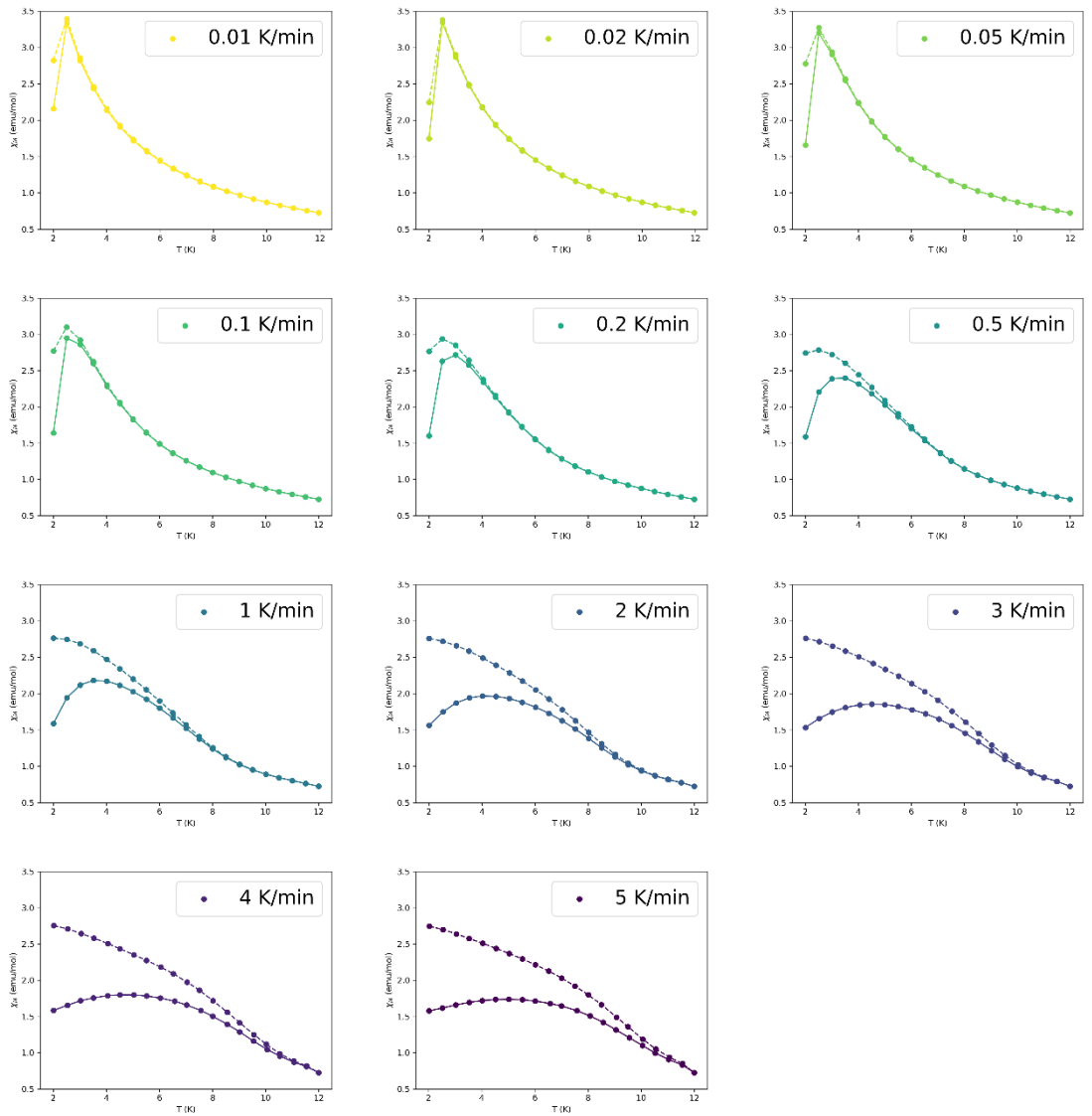


Figure S5. Temperature dependence of χ_M at ZFC and FC conditions with an applied field of 50 Oe and different heating rates.

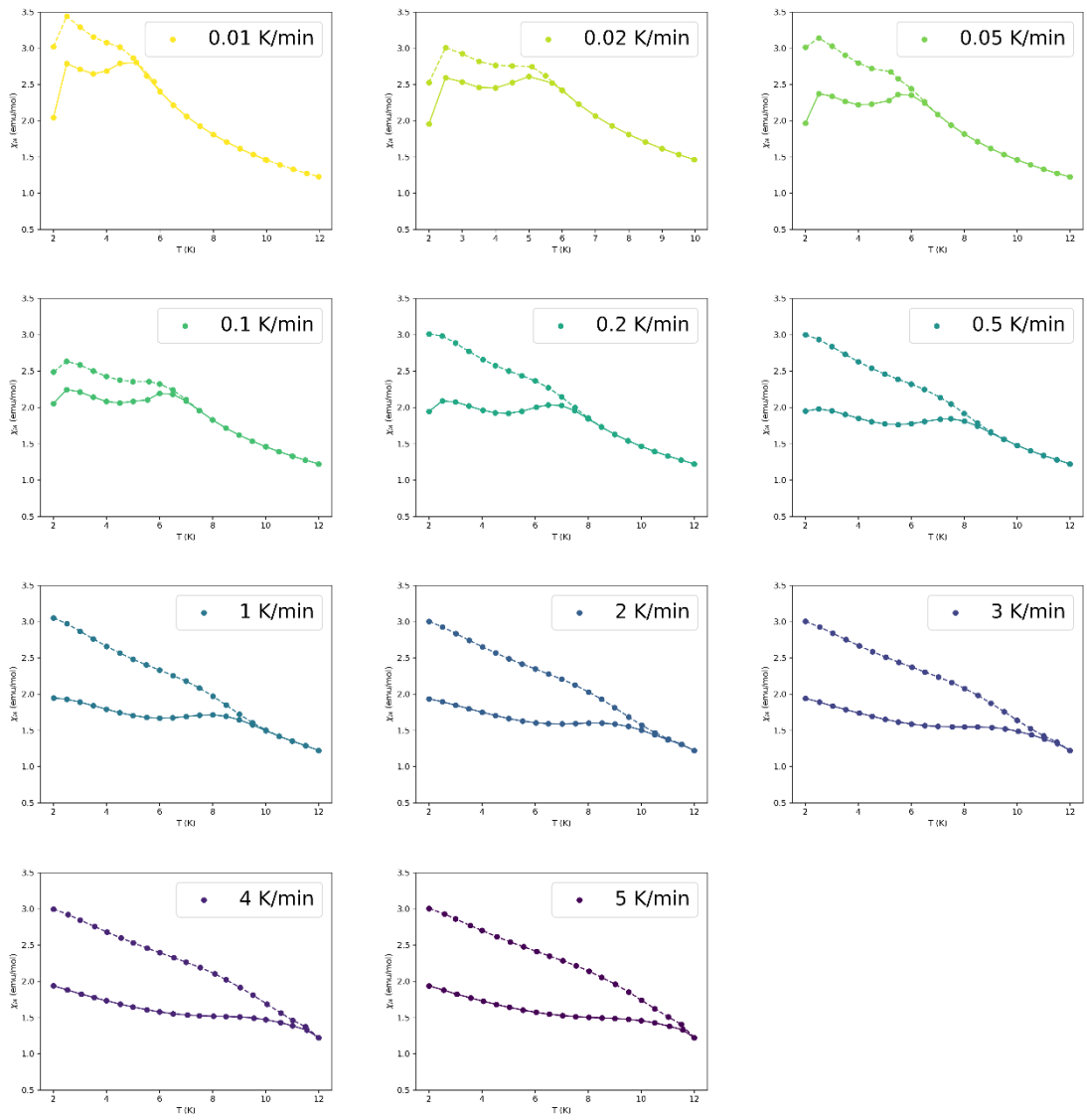


Figure S6. Temperature dependence of χ_M at ZFC and FC conditions with an applied field of 500 Oe and different heating rates. The double peaks at low temperatures, especially at low heating rates, have also been previously reported in magnetically diluted Er^{III} compounds.⁸ Such anomalous behaviour can be attributed to a secondary relaxation process at very low temperature.

Table S4. ZFC/FC blocking temperatures for different heating rates 0.01-5 K/min and applied DC fields of 50 Oe and 500 Oe.

Heating rate (K/min)	T _{B-ZFC/FC} (50 Oe) (K)	T _{B-ZFC/FC} (500 Oe) (K)
0.01	2.5	4.9
0.02	2.5	5.1
0.05	2.6	5.7
0.1	2.7	6.2
0.2	2.8	6.6
0.5	3.3	7.4
1	3.7	7.8
2	4.2	8.3
3	4.5	-
4	4.7	-
5	5.0	-

2.3. In-phase and out-of-phase magnetic susceptibility

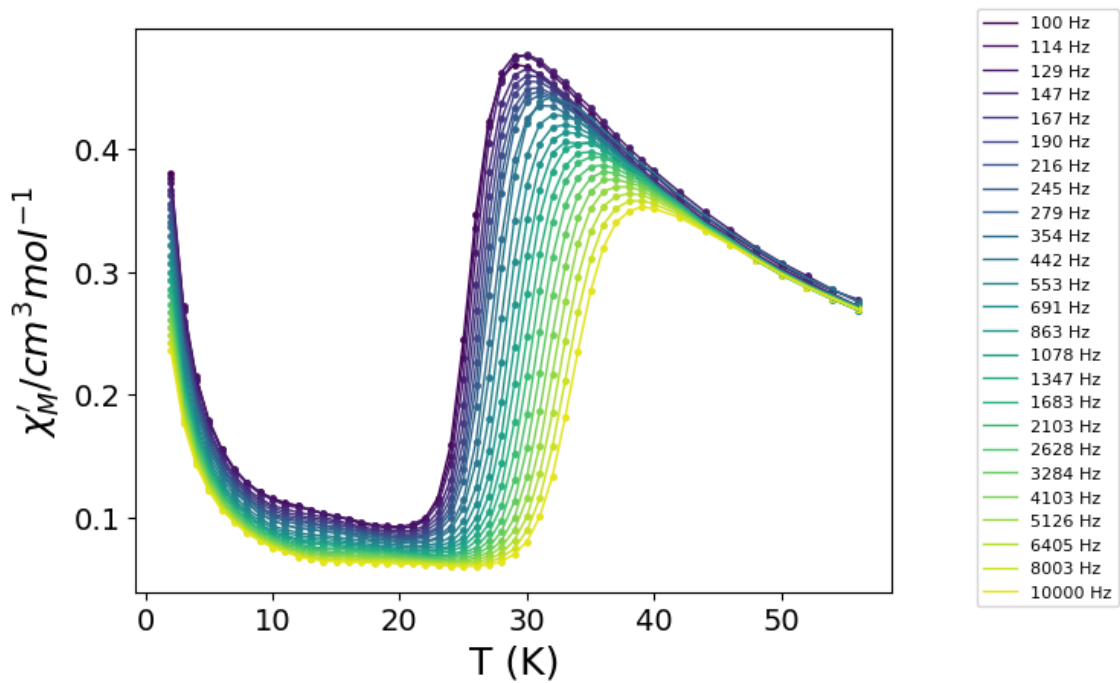


Figure S7. Temperature dependence of the in-phase ac magnetic susceptibility (χ'_M) under zero DC field for compound 1. The solid lines are a guide for the eye.

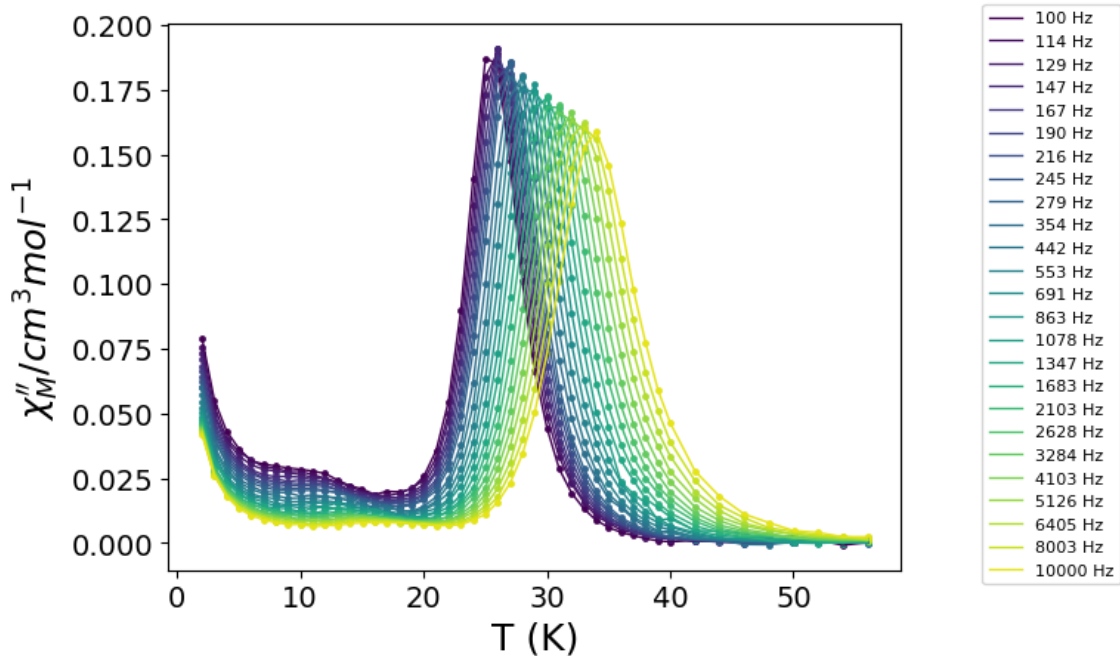


Figure S8. Temperature dependence of the out-of-phase ac magnetic susceptibility (χ''_M) under zero DC field for compound 1. The solid lines are a guide for the eye.

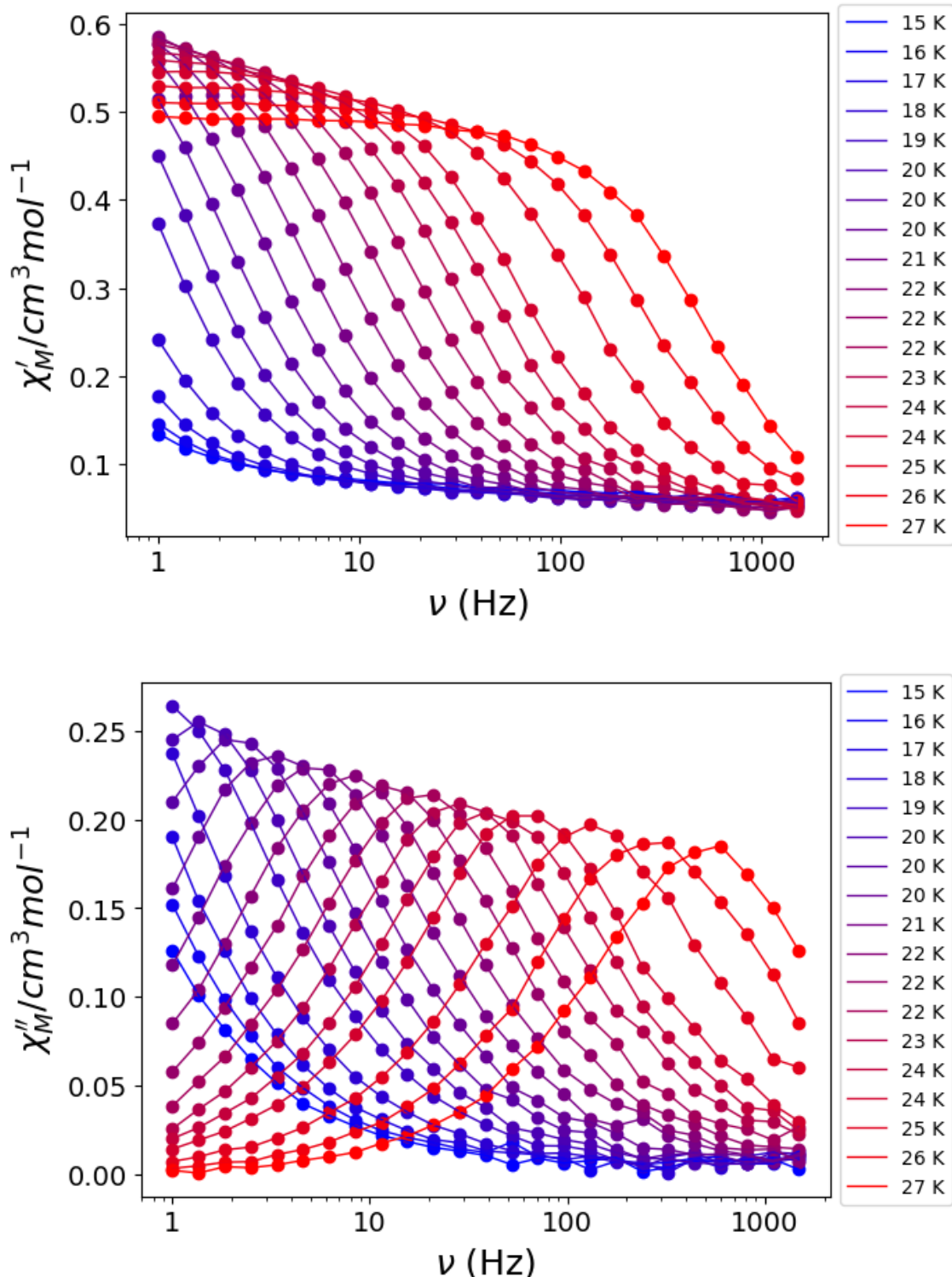


Figure S9. Frequency dependence of the in-phase (top) out-of-phase (bottom) component of the ac susceptibility (χ_M'') under zero DC field for compound **1**. The dots are connected with solid lines to improve visibility.

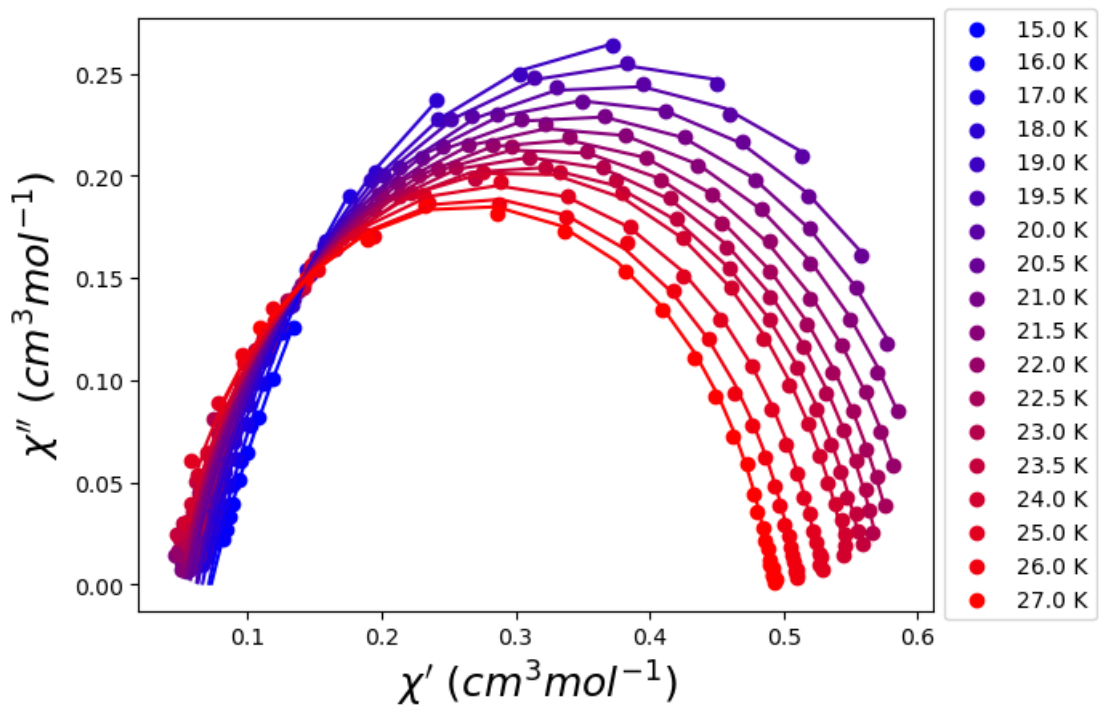


Figure S10. Cole-Cole plot χ_M'' vs. χ_M' plot for compound **1** under zero DC field at the indicated temperatures. The solid lines correspond to the best fit to the generalised Debye model

Table S5. Obtained values from the fit of the Cole-Cole plots shown in Figure S10.

T (K)	χ_s	χ_T	$\ln(\tau)$	α
15	0.073	1.328	1.006	0.223
16	0.071	1.060	0.355	0.192
17	0.066	0.944	-0.147	0.188
18	0.063	0.797	-0.850	0.179
19	0.062	0.678	-1.703	0.154
19.5	0.062	0.639	-2.141	0.145
20	0.057	0.629	-2.556	0.159
20.5	0.056	0.601	-3.017	0.151
21	0.054	0.584	-3.464	0.152
21.5	0.051	0.570	-3.903	0.153
22	0.050	0.552	-4.344	0.150
22.5	0.050	0.537	-4.766	0.145
23	0.048	0.527	-5.181	0.147
23.5	0.047	0.515	-5.581	0.146
24	0.048	0.502	-5.966	0.137
25	0.043	0.487	-6.711	0.139
26	0.041	0.468	-7.396	0.136
27	0.042	0.450	-8.039	0.122

2.4 Magnetisation decay

Table S6. Obtained values from the fit of the isothermal magnetisation decay using Eq. S1.

T (K)	M _{eq} (μ_B)	M ₀ (μ_B)	ln(τ)	β
2	-0.005622	0.227250	4.946	0.744
2.5	-0.005858	0.223989	4.963	0.745
3	-0.005829	0.204357	4.982	0.753
4	-0.003196	0.194385	4.888	0.759
5	-0.004583	0.148303	4.806	0.798
6	-0.003978	0.113889	4.547	0.849
7	-0.003241	0.055059	4.219	0.929
8	-0.003026	0.019242	3.763	0.973

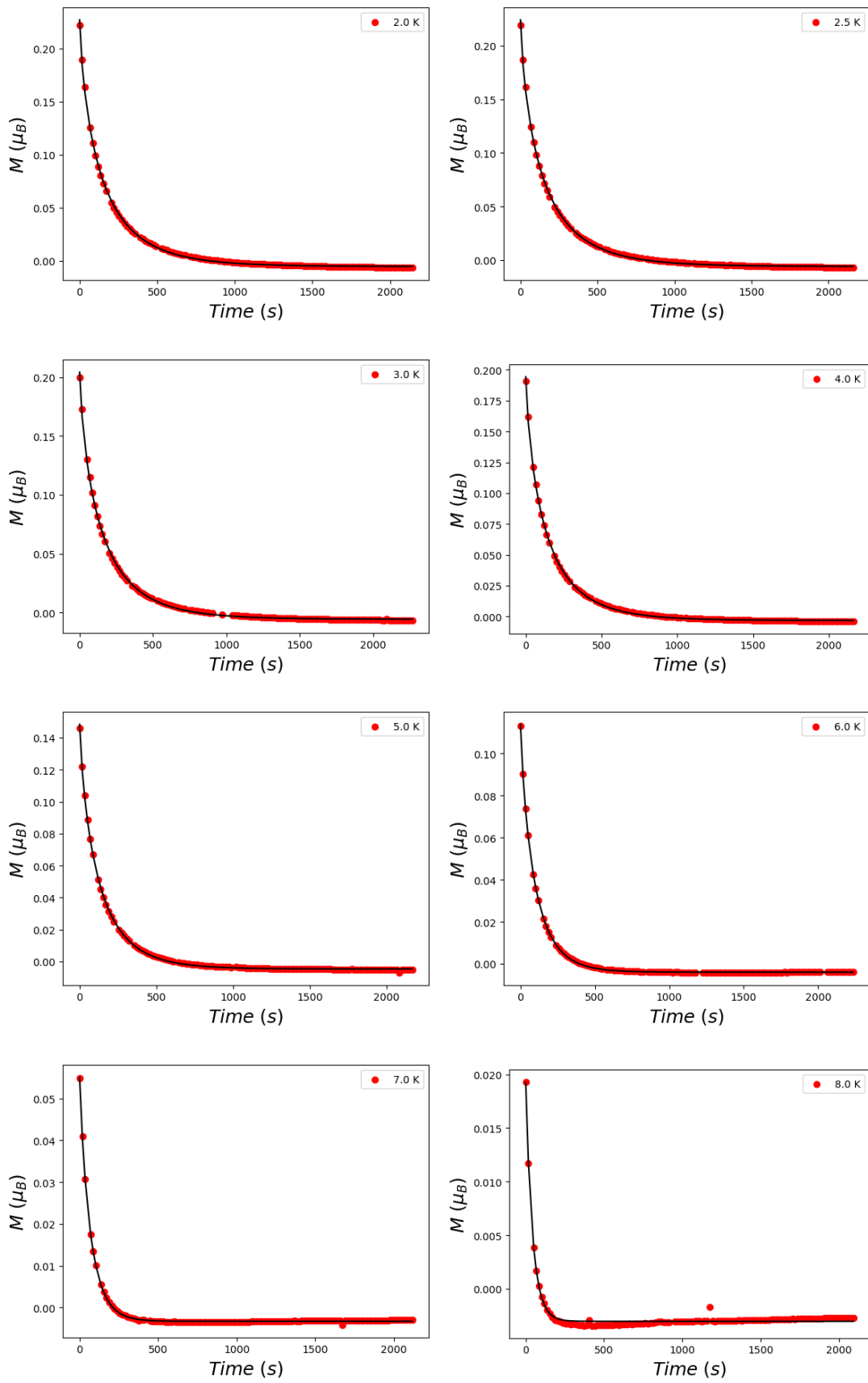


Figure S11. Isothermal magnetisation decay plots between 2 and 8 K. The black line is the fit using Eq. S1.

4. *Ab initio* calculations

Post–Hartree–Fock *ab initio* calculations were carried out on the crystal structure of **1**. For the calculations, two quantum chemistry program packages have been employed, Orca 5.0.3⁹⁻¹¹ and OpenMolcas 18.09.¹²⁻¹⁴ The electronic structure and magnetic properties have been computed using state-averaged complete active space self-consistent field calculations (SA-CASSCF (9,7)).¹⁵ The employed active space includes nine electrons in seven 4f orbitals of Dy^{III} CAS (9,7). Within this active space, we have computed 21 sextets states, 128 quadruplets and 98 doublets. For Orca quantum chemistry package, the spin-orbit effects were included using the quasi-degenerate perturbation theory (QDPT).¹⁶ Scalar relativistic effects were considered by second-order Douglas–Kroll–Hess (DKH) procedure.^{17, 18} In these calculations, all the atoms are described by the def2-TZVPP basis set,^{19, 20} including the corresponding auxiliary basis sets for correlation and Coulomb fitting for all the atoms apart from Dysprosium, for which the SARC2-DKH-QZVP basis set²¹ was used to take into account the relativistic effect. For OpenMolcas quantum chemistry package, the effect of spin–orbit coupling was considered perturbatively in a second step by using the restricted active space state interaction method (RASSI). Dynamic correlation contributions are not essential due to the relatively large ionic character of the Ln–O bonds. The MOLCAS ANO-RCC basis set²²⁻²⁴ was used for all the atoms. The following contractions were used: Dy [9s8p6d4f3g2h]; Br [5s4p2d]; P [5s4p3d2f]; O [4s3p2d1f]; C [3s2p] and H [2s]. In both program packages, the Single Aniso²⁵ approach was also used, which enables calculations of anisotropic magnetic properties and g tensors for the ground and first excited Kramers doublets (KD) and the matrix elements of the transition magnetic moments, which gives an estimation of the probability of transition between two different states of the molecules.²⁶

Table S7. CASSCF (ORCA) and CASSCF+RASSI (OpenMOLCAS) computed relative energies (in cm^{-1}) of the eight low-lying Kramers' doublets, g tensors and tilting angle (θ) of the main anisotropy axes (g_z component) of the corresponding excited (ES1, ES2, etc.) KD with respect to the ground state (GS) KD for **1**. ORCA and OpenMOLCAS results are given.

a) ORCA

Energy (cm^{-1})	g_{xx}	g_{yy}	g_{zz}	$\theta (\text{°})$
0.0	0.0008	0.0008	19.859	
275.2	0.129	0.274	16.920	6.4
336.6	0.419	1.634	17.732	90.0
406.7	2.673	8.120	8.263	77.5
445.6	1.163	2.993	13.167	32.3
467.1	0.067	1.183	7.623	0.9
526.5	2.224	2.326	11.701	39.1
674.4	0.004	0.022	18.945	58.4

b) OpenMOLCAS

Energy (cm^{-1})	g_{xx}	g_{yy}	g_{zz}	$\theta (\text{°})$
0.0	0.0008	0.0008	19.870	
277.5	0.116	0.227	16.967	6.4
345.6	0.484	1.820	17.620	90.0
412.3	8.263	7.766	2.674	12.5
449.8	1.085	2.807	13.199	31.6
473.6	0.432	1.578	7.767	4.1
531.2	2.419	2.680	11.415	37.4
674.9	0.002	0.028	18.921	58.3

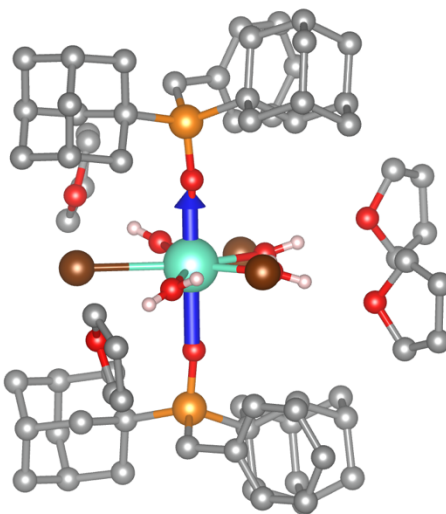


Figure S12. CASSCF+RASSI calculated anisotropy axis for the ground Kramers' doublet of complex **1** using OpenMOLCAS. Code colours: dysprosium (cyan), oxygen (red), bromide (brown), phosphorus (orange), and carbon (grey).

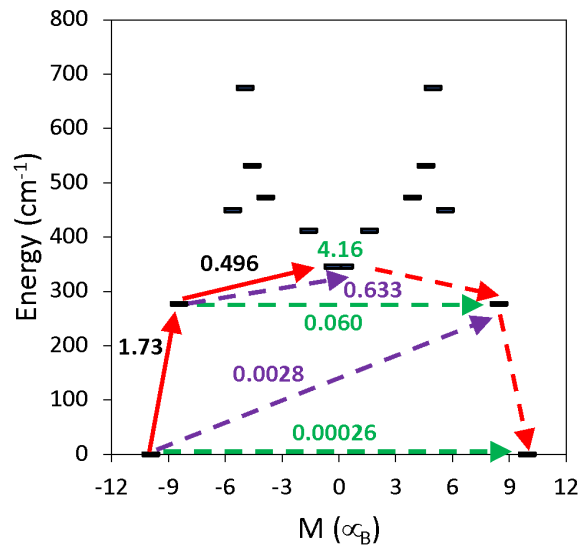


Figure S13. State energies as a function of their average magnetic moment, M , along the main anisotropy axis for **1** obtained with Single Aniso module from CASSCF+RASSI (OpenMOLCAS) calculations. The dashed green arrows correspond to the quantum tunnelling mechanism of ground or excited states, dashed purple arrow shows the hypothetical Orbach relaxation process. The solid red arrow indicates the transition between the ground and excited Kramers' doublets, and the dashed red arrow indicates the excitation pathway to the ground state with the reversed spin. The values close to the arrows indicate the matrix elements of the transition magnetic moments (above 0.1, an efficient spin relaxation mechanism is expected).

4. Theoretical Model

Comparison between Eqs. 7 and 13

The effect of the Curie law approximation inherent to Eq. 13 and the best choice for C_1' are evaluated by comparing the blocking temperatures predicted by Eqs. 13 and 7 for selected experimental cases. Four systems were chosen among the literature data presented in Table S9, as they have shown significant deviations from the Curie law in the χT plot, even at temperatures as high as 50K. The selected molecules were number 2 (refcode: LIRQUB), 4 (BAWLOD), 38 (VAGMOJ) and 43 (EHEHOR).

Eq. 7 from the main text is presented as:

$$\chi_{ZFC} = \chi_T \left[-C'_1 \exp \left(-R_H^{-1} \int \tau^{-1} dT \right) + 1 \right] = \lambda \chi_T$$

Where χ_T is the temperature-dependent susceptibility, digitalised from the reported $\chi^* T$ plots. Eq. 13 corresponds to:

$$T_B = \frac{R_H \left[1 - C'_1 \exp \left(-R_H^{-1} \int_0^{T_B} \tau^{-1} dT \right) \right]}{C'_1 \exp \left(-R_H^{-1} \int_0^{T_B} \tau^{-1} dT \right) \tau^{-1}(T_B)}$$

Thus, we calculated the blocking temperature for the four selected cases using Eqs. 13 and 7 for C_1' values ranging from 1 to 0.1 (See Table S8). For the results derived from Eq. 7, the experimental χT plot was digitized from published data to interpolate the χ_T function avoiding the Curie Law approximation.

Table S8. Experimental and calculated ZFC/FC blocking temperatures using Eqs. 7 and 13. Missing values for $T_{B-ZFC/FC}$ correspond to ZFC curves without a discernible maximum.

N°	REFCODE	$T_{B-ZFC/FC}$ (exp,K)	C1'	$T_{B-ZFC/FC}$ (calc. eq 8, K)	$T_{B-ZFC/FC}$ (calc. eq 13, K)
2	LIRQUB	55	1.0	57.0	55.8
			0.9	56.0	54.6
			0.8	54.9	53.1
			0.7	53.5	51.1
			0.6	51.7	47.7
			0.5	49.2	-
			0.4	45.5	-
			0.3	21.0	-
			0.2	20.9	-
			0.1	20.8	-
4	BAWLOD	45	1.0	51.3	50.5
			0.9	50.5	49.8
			0.8	49.4	49.0
			0.7	48.2	47.9
			0.6	46.8	46.4
			0.5	45.0	43.9
			0.4	42.3	-
			0.3	-	-
			0.2	-	-
			0.1	-	-
38	VAGMOJ	6.4	1.0	6.3	6.3
			0.9	6.3	6.3
			0.8	6.3	6.3
			0.7	6.3	6.2
			0.6	6.3	6.2
			0.5	6.2	6.2
			0.4	6.2	6.2
			0.3	6.2	6.2
			0.2	6.2	6.1
			0.1	6.1	-
43	EHEHOR	5.5	1.0	5.3	4.8
			0.9	5.3	4.7
			0.8	5.3	4.6
			0.7	5.3	4.5
			0.6	5.2	4.3
			0.5	5.2	4.0
			0.4	5.2	-
			0.3	5.2	-
			0.2	5.1	-
			0.1	5.1	-

ZFC/FC curves for Tunneling, Orbach and Raman relaxation

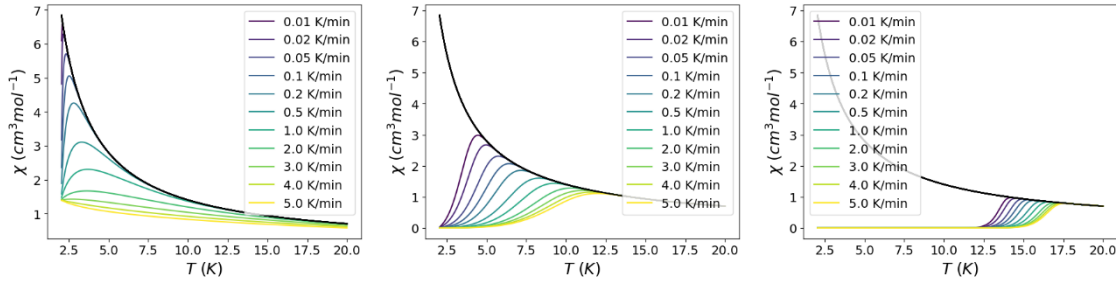


Figure S14. ZFC/FC curves simulated from Eq. 7 for the different demagnetisation mechanisms. (left) Tunnelling, (centre) Raman and (right) Orbach.

5. Model Assessment

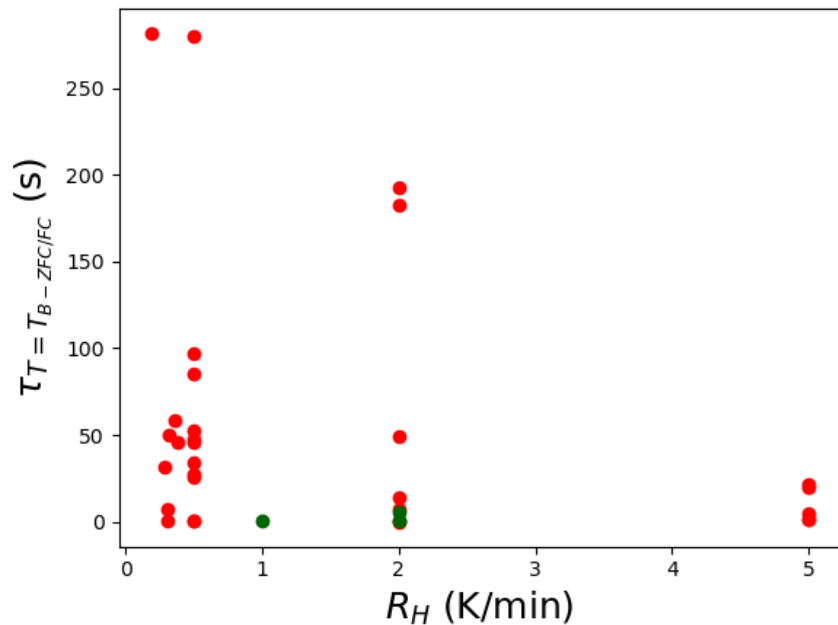


Figure S15. Relaxation time (s) at the ZFC/FC blocking temperature for the systems presented in Table S9 (red and green for lanthanide and transition metal compounds, respectively). Data is presented as a function of the heating rate (K/min).

Table S9. Experimental demagnetisation parameters and ZFC/FC blocking temperatures for literature examples of SMMs. The estimation of T_B based on Eq. 13 is presented employing the experimentally reported heating rate. In the cases where no heating rate is reported, the ZFC/FC blocking temperature was calculated assuming a slow and fast heating rate (0.2 K/min and 5 K/min, respectively). For the ZFC/FC section, R_H corresponds to the heating rate, $\mu_0 H$ is the static magnetic field and τ is the relaxation time at the temperature of $T_{B-ZFC/FC}$. For the demagnetisation parameters, τ_0 and U_{eff} are the Orbach prefactor and effective demagnetisation barrier, respectively, C and n are the usual Raman parameters and T_{QTM} is the tunnelling relaxation time.

	Compound	REFCODE	Eq.13		ZFC/FC				T_{B-100} (K)	Demagnetisation parameters					Ref.
			R_H (K min ⁻¹)	T_B (K)	R_H (K min ⁻¹)	T_{B-ZFC} (K)	$\mu_0 H$ (T)	τ (s)		τ_0 (s)	U_{eff} (K)	C (s ⁻¹ K ⁻ⁿ)	n	T_{QTM} (s)	
Dy^{III} complexes															
1	(Cp ^{iPr₅}) ₂ Dy ₂ I ₃	-	0.2 5	71.5 78.7	-	75	0.1	229	72	6.31×10^{-13}	2346.7 6	-	-	-	27
2	[K(2.2.2)][[1-(piperidino)-2,3,4,5-tetraphenylboroly]Dy]	TERGIK	0.2 5	21.2 64.0	-	68*	-	89.7	66	2.01×10^{-13}	2385.61	2.4×10^{-6}	1.93	-	28
3	[(η ⁵ -Cp*)Dy(η ⁵ -Cp ^{iPr₅})] [B(C ₆ F ₅) ₄]	LIRQUB	2	55.8	2	55 ^a 78*	0.1	192	65	4.2×10^{-12}	2217.27	3.1×10^{-8}	3	2.5×10^4	29
4	[(Cp ^{III}) ₂ Dy][B(C ₆ F ₅) ₄]	MEKDOI	0.2 5	20.0 60.4	-	61*	0.1	152.05	53	1.99×10^{-11}	1759.71	1.66×10^{-6}	2.151	-	30
5	[(Cp ^{III}) ₂ Dy][B(C ₆ F ₅) ₄]	BAWLOD	2	50.5	2	45	0.1	182.68	53	1.09×10^{-11}	1807	1.81×10^{-9}	3.92	-	31
6	[(Cp ^{III}) ₂ Dy _{0.08} Y _{0.92}][B(C ₆ F ₅) ₄]	BAWLOD	0.2 5	18.0 62.7	-	45	0.1	181.18	-	2.06×10^{-11}	1753.95	4.29×10^{-6}	1.88	-	30
7	[Dy(Cp ^{iPr₅} Me) ₂][B(C ₆ F ₅) ₄]	WIRHIR	0.2 5	21.7 62.6	-	65*	0.1	219.40	62	4.01×10^{-12}	2121.23	1.57×10^{-6}	2.07	2.45×10^3	32
8	[Dy(Cp ^{iPr₅}) ₂] [B(C ₆ F ₅) ₄]	WIRGUC	0.2 5	22.2 59.1	-	60*	0.1	162.83	56	1.18×10^{-11}	1919.42	8.04×10^{-7}	2.31	1.19×10^3	

9	[Dy(Cp <i>i</i> Pr ₂ Et) ₂][B(C ₆ F ₅) ₄]	WIRHEN	0.2 5	30.6 69.7	-	60*	0.1	292.64	59	7.79×10 ⁻¹²	1985.61	3.36×10 ⁻⁸	3.02	4.47×10 ²	
10	[Dy(Dtp) ₂][Al{OC(CF ₃) ₃ } ₄]	DUBKET	0.2 5	8.8 40.3	-	25	0.1	289.9	23	1×10 ⁻¹²	1760	1×10 ⁻⁴	1.1	-	33
11	[Dy(L ⁻) ₂ (py) ₅][BPh ₄] ⁺	LOWZIJ	2	22.6	2	23	0.2	48.89	-	1.3×10 ⁻¹²	1625.9	1×10 ⁻⁷	3.9	-	34
12	Dy ₂ @C80(CH ₂ Ph)	FAWYOU	5	22.7	5	21.9	0.2	4.78	18.2	3.6×10 ⁻¹²	613	8.2×10 ⁻¹⁰	4.9	3.26×10 ³	35
13	Dy(OSiMe ₃) ₂ (4-MePy) ₅] ⁺	JUQDEH	0.5	10.9	0.5	16	0.2	27.87	11.1	3.02×10 ⁻¹²	1497.84	1.66×10 ⁻⁶	3.6	-	36
14	Dy(OSiMe ₃) ₂ (py) ₅] ⁺	JUQDAD	0.5	12.6	0.5	15	0.2	52.24	12.9	1.55×10 ⁻¹²	1595.68	2.88×10 ⁻⁷	4.1	-	36
15	Dy(OCMe ₃) ₂ (py) ₅] ⁺	RAPDUK01	0.5	11.0	0.5	14	0.2	46.13	10.9	1.38×10 ⁻¹²	1805.75	1.62×10 ⁻⁶	3.6	-	36
16	[Dy(O <i>i</i> Bu) ₂ (py) ₅][BPh ₄]	RAPDUK	0.2 5	9.3 18.3	-	14	0.2	47.76	-	1.17×10 ⁻¹²	1815	1×10 ⁻⁶	3.77	-	37
17	Dy(OPh) ₂ (py) ₅] ⁺ †	JUQGAG	0.5	13.3	0.5	13	0.2	97.47	13.1	1.74×10 ⁻¹²	1197.12	2.14×10 ⁻⁸	5.1		36
18	[Dy(SCS) ₂][K(2,2,2-cryptand)]	EPAHOV	0.36	9.9	0.36	13	0.1	58.23	12	2.04×10 ⁻¹²	1109	4.07×10 ⁻⁶	3.2	446.7	38
19	{[Dy(Cp [*]) ₂ (μ-Me ₃ AlNEt ₃) ₂]2}[Al{OC(CF ₃) ₃ } ₄] ₂	HULRAK	0.2 5	9.3 16.6	-	12.5 (22*)	0.1	343.89	-	2.51×10 ⁻¹²	1230	2.51×10 ⁻⁷	4.5	-	39
20	[Dy(SCS) ₂ (K(DME) ₂) ₂]	EPAGOU	0.38	9.6	0.38	12	0.1	46.32	8	1.62×10 ⁻¹²	1160	2.75×10 ⁻⁶	3.5	195	38
21	Dy(OPh) ₂ (THF) ₅] ⁺	JUQFUZ	0.5	10.2	0.5	12	0.2	47.13	10	4.9×10 ⁻¹²	1329.5	1.02×10 ⁻⁶	4	-	36
22	{[L ₂ Dy(H ₂ O) ₅][Br] ₃ ·L ₂ ·H ₂ O}, L: 'BuPO(NH <i>i</i> Pr) ₂]	NAPDOB	2	10.8	2	11.6	-	13.79	-	1.1×10 ⁻¹¹	640	7.2×10 ⁻⁷	4.7	-	40
23	[Dy(Cp ^{III})(Cp [*])(PhF-κ-F)][Al{OC(CF ₃) ₃ } ₄]	-	0.2 5	6.1 14.0	-	11	-	38.38	8	2.19×10 ⁻¹²	1582.73	3.16×10 ⁻⁵	2.8	-	41
24	[Dy(Cp ^{III})(Cp [*])(PhCl-κ-Cl)][Al{OC(CF ₃) ₃ } ₄]	-	0.2	6.3	-	11	-	45.26	8	2.95×10 ⁻¹²	1618.70	2.95×10 ⁻⁵	2.76		41

			5	14.6												
25	[Dy(SCS) ₂][Na(DME) ₃]	EPAHAH	0.32	9.0	0.32	11	0.1	50.43	8	1.51×10 ⁻¹²	1015	2.95×10 ⁻⁶	3.54	182	38	
26	Dy(CyPh ₂ PO) ₂ (H ₂ O) ₅]·(PMo ₁₂ O ₄₀)·3CyPh ₂ PO·H ₂ O	-	0.2 5	6.2 9.9	-	9	0.1	9.5	6	2.6×10 ⁻¹¹	449	3.12×10 ⁻⁷	5.8	-	42	
27	[Dy(NCN) ₂][K(DB18C6)(THF)(toluene)]	EPAJAJ	0.28	8.5	0.28	10	0.1	32.06	-	2.95×10 ⁻¹²	757	6.02×10 ⁻⁷	4.49	79.43	38	
28	[Dy(BIPM ^{TMS}) ₂][K(18C6) (THF) ₂] †	RUXCUK	0.189	11	0.189	10	0.1	281.69	12	5.65×10 ⁻¹³	813	3.55×10 ⁻⁹	6	-	43	
29	Dy(bbpen-CH ₃)Br]	FICBOL	0.2 5	2.8 5.9	-	8.8	0.2	1.98	-	1.02×10 ⁻¹²	1162	5.35×10 ⁻⁴	3.15	-	44	
30	(PPh ₄)[Dy ₂ (bbpen) ₂ {Co(CN) ₆ }] · 3.5MeCN	POYJIZ	2	6.1	2	8.5	0.2	0.40	-	5.7×10 ⁻¹³	1065	1.2×10 ⁻⁴	3.46	0.43	45	
31	[Dy _{0.05} Y _{0.95} (bbpen)Br]	IMOTUB	0.2 5	4.6 8.5	-	8.3	0.2	7.89	-	2.71×10 ⁻¹³	1191	1.75×10 ⁻⁵	4.2	-	46	
32	[Dy(bbpen)Br]	IMOTUB	0.2 5	3.5 7	-	8 (9.5*)	0.2	4.63	-	1.51×10 ⁻¹²	1088	1.49×10 ⁻⁴	3.5	-	46	
33	{[L ₂ Dy(H ₂ O) ₅][Cl] ₃ ·L ₂ }, L: ¹ BuPO(NH <i>i</i> Pr) ₂	NAPDAM	2	7.3	2	8.2	-	7.8	-	4.4×10 ⁻¹²	624	6.5×10 ⁻⁶	4.7	-	40	
34	[K(crypt-222)][(Cp ^{Me4H₂} Dy) ₂ (μ-N ₂)]	LEPGIZ	0.2 5	6.9 8.6	-	7.5	1	14.69	6.6	1.7×10 ⁻⁸	155.54	2.1×10 ⁻⁶	4.13	6.7×10 ²	47	
35	Dy(OCMe ₃)(Cl)(THF) ₃] ⁺	ZIFPIQ01	0.5	7.7	0.5	7	0.2	0.70	-	4.36×10 ⁻¹²	938.13	1.78×10 ⁻⁶	4.5	0.708	36	
36	DyScS@C ₈ (6)-C ₈₂	XAJLAZ	5	7.8	5	7.3	0.3	20.12	5.4	5.3	9.78	-	-	-	48	
37	DyScS@C ₃ (8)-C ₈₂	XAJLED	5	6.2	5	7.3	0.3	21.17	4.9	11.3	4.60	-	-	-		
38	Dy(OPh)(Cl)(THF) ₃] ⁺	JUQFOT	0.5	5.8	0.5	6.8	0.2	25.51	5.1	4.47×10 ⁻¹¹	736.7	1.51×10 ⁻⁵	4.1	-	36	
39	[(Cp [*] ₂ Dy) ₂ (μ-bpym [•])](BPh ₄)	YEZBOW	0.2 5	6.6 7.8	-	6.5	-	28.41	-	1.03×10 ⁻⁷	126.33	-	-	2385.6	29	
40	[(Cp [*] ₂ Dy) ₄ (tz) ₄]·3(C ₆ H ₆) †	VAGMOJ	0.3	6.3	0.3	6.4	0.1	7.67	-	1×10 ⁻⁸	130.94	-	-	-	49	

41	[Dy _{0.07} Y _{0.93} (DiMeQ) ₂ (H ₂ O)Cl ₃]	TOQDUB	0.3	2.8	0.3	6	0.01	0.96	-	-	-	4×10 ⁻⁴	4	1.9	50
42	[Dy(bbpen)(tpo) ₂][BPh ₄]	VORCUD	0.2 5	2.7 5.4	-	7*	0.2	0.48	-	1.73×10 ⁻¹²	944	3.88×10 ⁻⁴	3.69	0.64	51
43	[Dy(H ₃ L ^{1,2,4}) ₂]	IPULUD	2	4.4	2	6*	0.1	1.28	-	2.2×10 ⁻¹⁰	367.7	4.9×10 ⁻⁵	5.4	-	52
44	[Dy(L*)Cl(DMF)] _n	IROYUM	3	6.2	3	5.8*	0.05	6.96	-	2.03×10 ⁻¹¹	399	1.27×10 ⁻⁶	6.62	-	53
45	[Dy(Cy ₃ PO) ₂ (μ-I)(I) ₂] ₂ ·4C ₇ H ₈	EHEHOR	0.5	4.8	0.5	5.5 ^a (12*)	0.2	34.07	-	7.3×10 ⁻¹²	1323	1.04×10 ⁻⁴	3.31	-	54
46	[Dy ^{III} L ^{N6} R(L ₂) ₂](BPh ₄)	RARNIL	0.2 5	1.3 2.7	-	5.1 (13*)	0.1	0.09	-	3.10×10 ⁻¹²	1454.68	2.29×10 ⁻²	2.51	9.68×10 ⁻²	55
47	[Dy(O ^t Bu) ₂ (L) ₄] ⁺ , L = 4-pyrrolidin-1-ylpyridine	ZUZSEV	0.2 5	2.1 4.4	-	5	0.1	3.9	-	2.13×10 ⁻¹²	1810	1.94×10 ⁻³	3.08	0.17	56
48	[Dy(O ^t Bu)Cl(py) ₅]BPh ₄	-	0.2 5	5.4 12.1	-	5	0.1	212.68	-	5×10 ⁻¹²	896	4.21×10 ⁻⁵	2.93	-	42
49	Dy(OSiMe ₃)(Cl)(THF) ₅ * ⁺	JUQCIK	0.5	6.6	0.5	4.5	0.2	279.58	5.9	2.82×10 ⁻¹¹	801.44	6.46×10 ⁻⁶	4.2	-	36
50	Dy(OSiMe ₃)(Br)(THF) ₅ * ⁺	JUQCUW	0.5	6.1	0.5	4.5	0.2	0.81	-	1.07×10 ⁻¹¹	732.37	6.61×10 ⁻⁶	4.5	0.813	36
51	Dy(OCMe ₃)(Br)(THF) ₅ * ⁺	JUQCQ	0.5	5.2	0.5	4.5	0.2	85.73	3.2	1.7×10 ⁻¹¹	818.71	4.47×10 ⁻⁵	3.7	-	36
52	[Dy _{0.05} Y _{0.95} (μ-OH)(DBP) ₂ (THF)] ₂	OWOXAB	0.2 5	2.3 4.5	-	4.5 ^a	0.25	4.34	-	2.1×10 ⁻¹²	755	8.3×10 ⁻⁴	3.74	-	57
53	[Dy(μ-OH)(DBP) ₂ (THF)] ₂	OWOXAB	0.2 5	2.8 5.3	-	2.5 ^a	0.25	14.47	-	3.5×10 ⁻¹²	754	2.7×10 ⁻⁴	4	-	57
54	[(THF) ₃ (μ-H) ₃ Li] ₂ [(η ⁵ -C ₆ H ₄ (CH ₂) ₂ C ₂ B ₉ H ₉)Dy _{0.1} Y _{0.9} (η ² ;η ⁵ -C ₆ H ₄ (CH ₂) ₂ C ₂ B ₉ H ₉) ₂ Li]	ZUNHOI	0.2 5	3.0 6.1	-	6.4*	0.2	3.96	-	3.6×10 ⁻¹¹	804	3.4×10 ⁻⁴	3.4	5	58
55	[(THF) ₃ (μ-H) ₃ Li] ₂ [(η ⁵ -C ₆ H ₄ (CH ₂) ₂ C ₂ B ₉ H ₉)Dy{η ² ;η ⁵ -C ₆ H ₄ (CH ₂) ₂ C ₂ B ₉ H ₉ } ₂ Li]	ZUNHOI	0.2	2.2	-	6.2*	0.2	0.21	-	4×10 ⁻¹¹	804	1.7×10 ⁻³	2.93	0.22	58

			5	4.8												
56	[DyL ^{ON3} (C ₅ H ₁₀ NS ₂) ₂]	PUKFAF	0.2 5	1.4 2.5	-	5*	0.1	0.02	-	2.99×10 ⁻¹²	638	2×10 ⁻²	3.24	0.017	59	
57	[Dy(Cp ^{III})(Cp [*])(C ₆ H ₄ F ₂ -κ ² -F,F)][Al{OC(CF ₃) ₃ } ₄]	-	0.2 5	1.2 2.3	-	4	-	0.30	-	7.94×10 ⁻¹²	1223	4.57×10 ⁻²	2.24	0.437	41	
58	[Dy(O'Bu) ₂ (L) ₄] ⁺ , L = 1,4-piperidin-1-ylpyridine	ZUZSIZ	0.2 5	2.3 5.2	-	4	0.1	14.63	-	1.36×10 ⁻¹²	1886	1.49×10 ⁻³	2.76	0.28	56	
59	[K(DME) _n][L ^A DyCl ₂]	JIZVIA	0.2 5	1.9 4.1	-	4	0.1	0.02	-	7×10 ⁻¹⁴	1334	3.01×10 ⁻³	3	0.023	60	
60	[K(DME) _n][L ^A DyI ₂]	DUXGUB	0.2 5	2.4 4.8	-	4	0.1	0.32	-	3.37×10 ⁻¹⁴	1278	9.89×10 ⁻⁴	3.35	0.33	60	
61	[(Cp [*]) ₂ Dy(NH ₃) ₂](BPh ₄)	KEPREF	0.2 5	1.3 2.6	-	4	0.1	0.86	-	2.6×10 ⁻¹²	785.61	0.022	2.86	2.8 ×10 ⁻³	61	
62	[Dy(pz) ₂ (THF) ₅][BPh ₄]	BADKUQ	0.2 5	1.4 2.5	-	4	0.2	0.10	-	9.05×10 ⁻¹²	521	2.1×10 ⁻²	3.01	0.12	60	
63	[Dy(pz) ₂ (py) ₅][BPh ₄]-2py	BADLAX	0.2 5	2.6 4.9	-	3.5	0.2	3.55	-	8.5×10 ⁻¹²	470	3.5×10 ⁻⁴	4.13	4.55		
64	[Dy(bbpen)NO ₃]	POYJAR	2	2.2	2	3.3	0.2	0.07	-	1.5×10 ⁻¹⁰	725	0.015	2.94	0.075	45	
65	[(Cp [*]) ₂ Dy(BPh ₄)]	-	0.2 5	1.5 3.0	-	3.2	0.1	2.78	-	2×10 ⁻⁸	448.92	0.009	3.17	0.0142	62	
66	[(C ₂ B ₉ H ₁₁) ₂ Dy _{0.09} Y _{0.91} (THF) ₂][Na(THF)]	ZUNGOH	0.2 5	2.8 5.1	-	3.2 ^a	0.2	0.2	-	1.27×10 ⁻⁹	430	1.9×10 ⁻⁴	4.46	0.20	58	
67	[Dy(L ₁) ₂ (THF) ₂][BPh ₄]	QILBUL	0.2 5	1.4 2.8	-	3.1	0.2	0.01	-	5×10 ⁻⁸	378.42	1.5×10 ⁻²	3	0.014	63	
68	[Dy(pz) ₂ (NS) ₅][BPh ₄]	BADLEB	0.2 5	1.7 3.1	-	3	0.2	0.47	-	8.2×10 ⁻¹²	444	4.9×10 ⁻³	3.77	0.55	62	
69	[Dy(Cy ₃ PO) ₂ I ₃ (CH ₃ CN)]	AJICOO	0.2 5	1.4 2.7	-	3 (7.4*)	0.2	2.30	-	5×10 ⁻¹²	1002	1.7×10 ⁻²	2.95	4.7 ×10 ⁻³	62	

70	[Dy _{0.19} Y _{1.81} (nb) ₄ (H ₂ L) ₂]	VANXOA	0.2 5	2.2 3.6	-	3 (3.9*)	0.1	0.29	-	1.15×10 ⁻¹¹	281.5	5.75×10 ⁻⁴	5.23	0.31	⁶⁴
71	[Dy _{0.10} Y _{1.90} (nb) ₄ (H ₂ L) ₂]	VANXOA	0.2 5	2.3 3.7	-	3 (4.2*)	0.1	0.45	-	1.07×10 ⁻¹¹	285	4.06×10 ⁻⁴	5.36	0.48	⁶⁴
72	[Dy(L ₂) ₂ (py) ₂][BPh ₄]	QILCAS	0.2 5	1.4 2.6	-	3	0.2	0.02	-	1.5×10 ⁻⁸	388.49	2×10 ⁻²	3	0.017	⁶³
73	[Dy ₂ (hfac) ₆ (NITThienPh) ₂] _n	KEVRUA01	0.2 5	2.5 2.8	-	3	0.005	0.076	-	1.73×10 ⁻⁹ 7.73×10 ⁻¹⁵	53 98	-	-	-	⁶⁵
74	[Dy ₃ (μ ₃ -CO ₃)(Clbbpen) ₃]·(CF ₃ SO ₃)·6MeCN	GUNDIF	2	3.7	2	4.2*	0.2	17.87	-	1.3×10 ⁻⁹	504	4.5×10 ⁻⁴	4.39	-	⁶⁶
75	[(Cp ⁺) ₂ Dy] ₂ (μ-tppz)][BPh ₄]	HOLJEZ	0.2 5	2.1 2.5	-	2.7	0.1	0.12	-	2.1×10 ⁻⁷	35.9	-	-	-	⁶⁷
76	[(C ₂ B ₉ H ₁₁) ₂ Dy(THF) ₂][Na(THF) ₅]	ZUNGOH	0.2 5	1.7 3.2	-	4.5*	0.2	0.01	-	1.2×10 ⁻⁹	430	5.5×10 ⁻³	3.5	0.015	⁵⁸
77	[Dy(L ^E)(4-MeOPhO) ₂](BPh ₄)·3THF	QORWAY	0.2 5	1.4 2.7	-	2.5 (6*)	0.2	0.13	-	1.85×10 ⁻¹²	1338	1.95×10 ⁻²	2.82	0.131	⁶⁸
78	[Dy(L ^E)(naPhO) ₂](BPh ₄)·4THF	QORWIG	0.2 5	1.6 3.2	-	2.5 (4*)	0.2	0.08	-	1.15×10 ⁻¹²	1226	7.1×10 ⁻³	3.2	0.085	⁶⁸
79	[Dy ^{III} (bpyN ₄)(Ph ₃ SiO) ₂](BPh ₄)	DIVBUJ	0.2 5	1.1 1.8	-	8.5*	0.2	1.54	-	3.52×10 ⁻⁸	584	1.18×10 ⁻¹	2.46	0.0288	⁶⁹
80	[Dy ₂ (L ^X) ₂ Cl ₂ (CH ₃ OH) ₃] _n ·nCH ₃ OH	IROYOG	3	3.3	3	2.4*	0.05	15.77	-	1.54×10 ⁻⁸	195	9.08×10 ⁻⁴	4.85	-	⁵³
81	[(L ^{CO})Dy(N ⁺) ₂]	PAXRIS	0.2 5	1.1 1.6	-	2.2	0.1	-	-	1.7×10 ⁻⁷	190	0.19	3.46	4.4×10 ⁻³	⁷⁰
82	Dy(bbpen-CH ₃ Cl)]	FICBIF	0.2 5	1.8 3.7	-	7*	0.2	0.11	-	2.36×10 ⁻¹⁰	723	4.6×10 ⁻³	2.97	0.11	⁴⁴
83	[Dy(acac) ₃ bpm]	FIKREA	1	2.5	1	3*	0.1	3.28	-	3.2×10 ⁻¹¹	309	1.4×10 ⁻³	4.9	4.5×10 ⁻³	⁷¹
84	[L ¹ Co(III)Br ₂ Dy(III)-(acac) ₂]·CH ₂ Cl ₂	CIHSUK	0.2	1.9	-	2	0.15	0.16	-	1.03×10 ⁻¹⁰	312.26	2.16×10 ⁻³	4.39	0.16	⁷²

				5	3.3													
85	[L ² Co(III)Cl ₂ Dy _{0.05} Y _{0.95} (acac)Cl(H ₂ O)]	CIHTEV	0.2 5	2.3 3.9	-	1.9	0.15	0.06	-	9.36×10 ⁻⁹	220.88	3.99×10 ⁻⁴	5.14	0.06	72			
86	[Cr ^{III} ₂ Dy ^{III} ₂ (OMe) ₂ (O ₂ CPh) ₄ (mdea) ₂ (NO ₃) ₂]	--	0.2 5	4.0 4.7	-	3.7	0.1	55.67	-	5.1×10 ⁻⁸	77	-	-	-	-	73		
87	[Dy ₃ Cr ₃ (μ ₃ -F)(μ ₃ -OH) ₃ (mdea) ₃ (piv) ₈ DMF] ·H ₂ O·CH ₃ CN	--	0.2 5	1.4 1.8	-	1.6	0.1	1.23	-	3×10 ⁻⁵	17	1.3×10 ⁻⁶	2	6×10 ⁷	74			
	Tb^{III} complexes																	
88	(Cp ^{iPr₅}) ₂ Tb ₂ I ₃	--	0.2 5	65.6 72.8	-	70	0.1	17.61	65	7.9×10 ⁻¹²	1989.9	-	-	-	-	27		
89	Tb ₂ @C80(CH ₂ Ph)	FAWYOU03	5	28.6	5	28.9	0.2	1.69	25.2	1.66×10 ⁻¹²	799	-	-	-	6.5×10 ⁴	75		
90	Tb ₂ @C79N	-	5	27.5	5	28	0.2	1.32	24.1	2.4×10 ⁻¹²	757	5.76×10 ⁻¹⁰	3.9	1.65×10 ⁴	76			
91	[K(crypt-222)][(Cp ^{Me₄H₂}) ₂ Tb] ₂ (μ-N ₂)]	LEPGEV	0.2 5	19.9 23.3	-	20	1	54.54	20	1.3×10 ⁻⁷	397.12	-	-	4×10 ⁴	47			
92	[K(crypt-222)(THF)][(Cp ^{Me₄H₂}) ₂ Tb(THF)] ₂ (μ-N ₂)]	LEPGUL	0.2 5	11.3 16.6	-	14.5	1	37.22	14	1.4×10 ⁻⁹	348.2	-	-	3.64×10 ³	47			
93	[K(18-crown-6)(THF)] ₂ [(Me ₃ Si) ₂ N] ₂ (THF)Tb] ₂ (μ-η ² :η ² -N ₂)	CAJRIQ	0.2 5	14.7 16.9	-	14	-	111.79	13.9	8.20×10 ⁻⁹	326.7	-	-	-	77			
94	[Cu ₃ Tb ₂ (Htris) ₂ (H ₂ tris) ₂ (NO ₃) ₆] _n ·2nC ₂ H ₅ OH	IJARAP	0.2 5	2.5 3.0	-	2.4	0.03	16.93	-	1.7×10 ⁻⁷	44.2	-	-	-	-	78		
	Er^{III} complexes																	
95	[Er _{0.05} Y _{0.95} (COT) ₂][K(18C6)]	YIWTUV01	0.2 5	10.9 12.7	-	10	0.1	162.97	-	6.9×10 ⁻⁸	215.83	-	-	-	-	79		
96	([Er-TiPS ₂ COT] ⁺) ₂ †	VEBHOD	0.2 5	5.6 8.4	-	5.4	0.01	81.95	-	2.60×10 ⁻¹⁰	198.56	1.50×10 ⁻⁷	6.7	-	-	80		
	Ho^{III} complexes																	
97	(Cp ^{iPr₅}) ₂ Ho ₂ I ₃	-	0.2	28.2	-	28	1	61.46	-	2.40×10 ⁻¹¹	800	-	-	-	-	81		

			5	31.4												
Transition Metal complexes																
98	[K(crypt-222)][Fe ^I (C(SiMe ₃) ₃) ₂]	-	0.2 5	4.0 7.2	-	4.5	0.1	44.23	-	6.91×10 ⁻¹⁰	342.8	2.27×10 ⁻⁵	4.59	-	-	82
99	[Fe ₄ (NC)Ph ₂) ₆]	-	1	2.2	-	2.2	0.05	0.63	-	9.1×10 ⁻⁹	39.7	-	-	-	-	83
100	Mn ₁₂ -BuCl	-	0.2 5	3.1 3.7	-	2.9	0.01	33.84	-	3.5×10 ⁻⁸	60	-	-	-	-	84
101	[Mn ₁₂ O ₁₂ (CH ₃ (CH ₂) ₁₆ CO ₂) ₁₁ (CH ₃ CO ₂) ₅ (H ₂ O) ₄]	-	0.2 5	3.4 4.3	-	3.0	0.1	63.6	-	1.03×10 ⁻⁴	40	-	-	-	-	85
102	[Mn ₁₂ O ₁₂ (CH ₃ (CH ₂) ₁₆ CO ₂) ₁₆]·2CH ₃ COOH·4H ₂ O immobilized (SiS-Mn12N1)	-	0.2 5	3.2 4.4	-	2.7	0.01	105.27	-	3.3×10 ⁻³	28	-	-	-	-	86
103	[Mn ₁₂ O ₁₂ (CH ₃ COO) ₁₆ (H ₂ O) ₄]·2CH ₃ COOH·4H ₂ O	-	0.2 5	3.1 3.5	-	3.4	0.1	130.15	-	7.76×10 ⁻¹¹	76	-	-	-	-	87
104	[Mn ₁₂ O ₁₂ (CN-o-C ₆ H ₄ CO ₂) ₁₂ (CH ₃ CO ₂) ₄ (H ₂ O) ₄] ·8CH ₂ Cl ₂ †	-	0.2 5	1.7 1.9	-	2.0	1	0.07	-	2×10 ⁻⁹	34.8	-	-	-	-	88
105	Co ₄ L ₄ ·0.5H ₂ O	-	0.2 5	1.9 2.2	-	4.5*	0.001	9×10 ⁻⁵	-	5.4×10 ⁻⁹	38.8	-	-	-	-	89
106	[L ₂ Co](TBA) ₂ †	-	2	2.4	2	3.5	0.5	0.69	-	1.46×10 ⁻¹⁰	325	4.92×10 ⁻³	4.54	-	-	90
107	Mn ₂ ^{II} Mo ^{III}	DOCVEY	2	3.3	2	3	0.0005	0.16		2.0 × 10 ⁻⁸	58.5	-	-	-	-	91

QTM values in italics were not considered to calculate T_B as they should be quenched by the static magnetic field to allow the observation of T_B in the ZFC/FC experiment.

† One process was used to calculate T_B .

* T_{irrev} .

^a Not explicitly informed in the article but estimated value from ZFC/FC curves.

6. References

1. (a) *APEX2*, Bruker AXS: Madison, 2010. (b) *SAINT*, 8.30a; Bruker AXS: Madison, 2013.
2. Sheldrick, G. M. *SADABS*, 2004/1; Bruker AXS: Madison, 2008.
3. G. M. Sheldrick, SHELXT Integrated space-group and crystal-structure determination, *Acta Crystallographica Section A Foundations and Advances*, 2015, **71**, 3-8.
4. G. M. Sheldrick, A short history of SHELX, *Acta Crystallographica Section A Foundations of Crystallography*, 2007, **64**, 112-122.
5. O. V. Dolomanov, L. J. Bourhis, R. J. Gildea, J. A. K. Howard and H. Puschmann, OLEX2: a complete structure solution, refinement and analysis program, *J. Appl. Crystallogr.*, 2009, **42**, 339-341.
6. D. Gatteschi, R. Sessoli and J. Villain, Molecular Nanomagnets, 2006, 108-159.
7. R. Orbach, On the Theory of Spin-Lattice Relaxation in Paramagnetic Salts, *Proc. Phys. Society*, 1961, **77**, 821-826.
8. A. P. Orlova, M. S. Varley, M. G. Bernbeck, K. M. Kirkpatrick, P. C. Bunting, M. Gembicky and J. D. Rinehart, Molecular Network Approach to Anisotropic Ising Lattices: Parsing Magnetization Dynamics in Er³⁺ Systems with 0–3-Dimensional Spin Interactivity, *Journal of the American Chemical Society*, 2023, 145, 22265-22275.
9. F. Neese, Software update: the ORCA program system, version 4.0, *WIREs Comput. Mol. Sci.*, 2018, **8**, e1327.
10. F. Neese, Software update: The ORCA program system—Version 5.0, *WIREs Comput. Mol. Sci.*, 2022, **12**, e1606.
11. F. Neese, F. Wennmohs, U. Becker and C. Riplinger, The ORCA quantum chemistry program package, *J. Chem. Phys.*, 2020, **152**, 224108.
12. G. Li Manni, I. Fdez. Galván, A. Alavi, F. Aleotti, F. Aquilante, J. Autschbach, D. Avagliano, A. Baiardi, J. J. Bao, S. Battaglia, L. Birnoschi, A. Blanco-González, S. I. Bokarev, R. Broer, R. Cacciari, P. B. Calio, R. K. Carlson, R. Carvalho Couto, L. Cerdán, L. F. Chibotaru, N. F. Chilton, J. R. Church, I. Conti, S. Coriani, J. Cuéllar-Zuquin, R. E. Daoud, N. Dattani, P. Decleva, C. de Graaf, M. G. Delcey, L. De Vico, W. Dobrutz, S. S. Dong, R. Feng, N. Ferré, M. Filatov, L. Gagliardi, M. Garavelli, L. González, Y. Guan, M. Guo, M. R. Hennefarth, M. R. Hermes, C. E. Hoyer, M. Huix-Rotllant, V. K. Jaiswal, A. Kaiser, D. S. Kaliakin, M. Khamesian, D. S. King, V. Kochetov, M. Krośnicki, A. A. Kumaar, E. D. Larsson, S. Lehtola, M.-B. Lepetit, H. Lischka, P. López Ríos, M. Lundberg, D. Ma, S. Mai, P. Marquetand, I. C. D. Merritt, F. Montorsi, M. Mörchen, A. Nenov, V. H. A. Nguyen, Y. Nishimoto, M. S. Oakley, M. Olivucci, M. Oppel, D. Padula, R. Pandharkar, Q. M. Phung, F. Plasser, G. Raggi, E. Rebolini, M. Reiher, I. Rivalta, D. Roca-Sanjuán, T. Romig, A. A. Safari, A. Sánchez-Mansilla, A. M. Sand, I. Schapiro, T. R. Scott, J. Segarra-Martí, F. Segatta, D.-C. Sergentu, P. Sharma, R. Shepard, Y. Shu, J. K. Staab, T. P. Straatsma, L. K. Sørensen, B. N. C. Tenorio, D. G. Truhlar, L. Ungur, M. Vacher, V. Veryazov, T. A. Voß, O. Weser, D. Wu, X. Yang, D. Yarkony, C. Zhou, J. P. Zobel and R. Lindh, The OpenMolcas Web: A Community-Driven Approach to Advancing Computational Chemistry, *J. Chem. Theory Comput.*, 2023, **19**, 6933-6991.
13. I. Fdez. Galván, M. Vacher, A. Alavi, C. Angeli, F. Aquilante, J. Autschbach, J. J. Bao, S. I. Bokarev, N. A. Bogdanov, R. K. Carlson, L. F. Chibotaru, J. Creutzberg, N. Dattani, M. G. Delcey, S. S. Dong, A. Dreuw, L. Freitag, L. M. Frutos, L. Gagliardi, F. Gendron, A. Giussani, L. González, G. Grell, M. Guo, C. E. Hoyer, M. Johansson, S. Keller, S. Knecht, G. Kovačević, E. Källman, G. Li Manni, M. Lundberg, Y. Ma, S. Mai, J. P. Malhado, P. Å. Malmqvist, P. Marquetand, S. A. Mewes, J. Norell, M. Olivucci, M. Oppel, Q. M. Phung, K. Pierloot, F. Plasser, M. Reiher, A. M. Sand, I. Schapiro, P. Sharma, C. J. Stein, L. K. Sørensen, D. G. Truhlar, M. Ugandi, L. Ungur, A. Valentini, S. Vancoillie, V. Veryazov, O. Weser, T. A.

- Wesołowski, P.-O. Widmark, S. Wouters, A. Zech, J. P. Zobel and R. Lindh, OpenMolcas: From Source Code to Insight, *J. Chem. Theory Comput.*, 2019, **15**, 5925-5964.
14. F. Aquilante, J. Autschbach, A. Baiardi, S. Battaglia, V. A. Borin, L. F. Chibotaru, I. Conti, L. De Vico, M. Delcey, I. Fdez. Galván, N. Ferré, L. Freitag, M. Garavelli, X. Gong, S. Knecht, E. D. Larsson, R. Lindh, M. Lundberg, P. Å. Malmqvist, A. Nenov, J. Norell, M. Odelius, M. Olivucci, T. B. Pedersen, L. Pedraza-González, Q. M. Phung, K. Pierloot, M. Reiher, I. Schapiro, J. Segarra-Martí, F. Segatta, L. Seijo, S. Sen, D.-C. Sergentu, C. J. Stein, L. Ungur, M. Vacher, A. Valentini and V. Veryazov, Modern quantum chemistry with [Open]Molcas, *J. Chem. Phys.*, 2020, **152**, 214117.
 15. P.-Å. Malmqvist and B. O. Roos, The CASSCF state interaction method, *Chem. Phys. Lett.*, 1989, **155**, 189-194.
 16. D. Ganyushin and F. Neese, First-principles calculations of zero-field splitting parameters, *J. Chem. Phys.*, 2006, **125**, 024103.
 17. M. Douglas and N. M. Kroll, Quantum electrodynamical corrections to the fine structure of helium, *Annals Phys.*, 1974, **82**, 89-155.
 18. B. A. Hess, Applicability of the no-pair equation with free-particle projection operators to atomic and molecular structure calculations, *Phys. Rev. A*, 1985, **32**, 756-763.
 19. F. Weigend, Accurate Coulomb-fitting basis sets for H to Rn, *Phys. Chem. Chem. Phys.*, 2006, **8**, 1057-1065.
 20. F. Weigend and R. Ahlrichs, Balanced basis sets of split valence, triple zeta valence and quadruple zeta valence quality for H to Rn: Design and assessment of accuracy, *Phys. Chem. Chem. Phys.*, 2005, **7**, 3297-3305.
 21. D. Aravena, F. Neese and D. A. Pantazis, Improved Segmented All-Electron Relativistically Contracted Basis Sets for the Lanthanides, *J. Chem. Theory Comput.*, 2016, **12**, 1148-1156.
 22. P.-O. Widmark, P.-k. Malmqvist and B. r. O. Roos, Density matrix averaged atomic natural orbital (ANO) basis sets for correlated molecular wave functions, *Theor. Chim. Acta*, 1990, **77**, 291-306.
 23. B. O. Roos, R. Lindh, P.-Å. Malmqvist, V. Veryazov, P.-O. Widmark and A. C. Borin, New Relativistic Atomic Natural Orbital Basis Sets for Lanthanide Atoms with Applications to the Ce Diatom and LuF₃, *J. Phys. Chem. A*, 2008, **112**, 11431-11435.
 24. B. O. Roos, R. Lindh, P.-Å. Malmqvist, V. Veryazov and P.-O. Widmark, Main Group Atoms and Dimers Studied with a New Relativistic ANO Basis Set, *J. Phys. Chem. A*, 2003, **108**, 2851-2858.
 25. L. F. Chibotaru and L. Ungur, Ab initio calculation of anisotropic magnetic properties of complexes. I. Unique definition of pseudospin Hamiltonians and their derivation, *J. Chem. Phys.*, 2012, **137**, 064112.
 26. L. Ungur and L. F. Chibotaru, Strategies toward High-Temperature Lanthanide-Based Single-Molecule Magnets, *Inorg. Chem.*, 2016, **55**, 10043-10056.
 27. C. A. Gould, K. R. McClain, D. Reta, J. G. C. Kragskow, D. A. Marchiori, E. Lachman, E.-S. Choi, J. G. Analytis, R. D. Britt, N. F. Chilton, B. G. Harvey and J. R. Long, Ultrahard magnetism from mixed-valence dilanthanide complexes with metal-metal bonding, *Science*, 2022, **375**, 198-202.
 28. J. C. Vanjak, B. O. Wilkins, V. Vieru, N. S. Bhuvanesh, J. H. Reibenspies, C. D. Martin, L. F. Chibotaru and M. Nippe, A High-Performance Single-Molecule Magnet Utilizing Dianionic Aminoborolide Ligands, *J. Am. Chem. Soc.*, 2022, **144**, 17743-17747.
 29. S. Demir, J. M. Zadrozny, M. Nippe and J. R. Long, Exchange Coupling and Magnetic Blocking in Bipyrimidyl Radical-Bridged Dilanthanide Complexes, *J. Am. Chem. Soc.*, 2012, **134**, 18546-18549.
 30. C. A. P. Goodwin, F. Ortú, D. Reta, N. F. Chilton and D. P. Mills, Molecular magnetic hysteresis at 60 kelvin in dysprosocenium, *Nature*, 2017, **548**, 439-442.

31. F.-S. Guo, B. M. Day, Y.-C. Chen, M.-L. Tong, A. Mansikkamäki and R. A. Layfield, A Dysprosium Metallocene Single-Molecule Magnet Functioning at the Axial Limit, *Angew. Chem. Inter. Ed.*, 2017, **56**, 11445-11449.
32. K. Randall McClain, C. A. Gould, K. Chakarawet, S. J. Teat, T. J. Groshens, J. R. Long and B. G. Harvey, High-temperature magnetic blocking and magneto-structural correlations in a series of dysprosium(III) metallocenium single-molecule magnets, *Chem. Sci.*, 2018, **9**, 8492-8503.
33. P. Evans, D. Reta, G. F. S. Whitehead, N. F. Chilton and D. P. Mills, Bis-Monophospholyl Dysprosium Cation Showing Magnetic Hysteresis at 48 K, *J. Am. Chem. Soc.*, 2019, **141**, 19935-19940.
34. K.-X. Yu, J. G. C. Kragskow, Y.-S. Ding, Y.-Q. Zhai, D. Reta, N. Chilton and Y.-Z. Zheng, Enhancing Magnetic Hysteresis in Single-Molecule Magnets by Ligand Functionalisation, *Chem.*, 2020, **6**, 1777–1793.
35. F. Liu, D. S. Krylov, L. Spree, S. M. Avdoshenko, N. A. Samoylova, M. Rosenkranz, A. Kostanyan, T. Greber, A. U. B. Wolter, B. Büchner and A. A. Popov, Single molecule magnet with an unpaired electron trapped between two lanthanide ions inside a fullerene, *Nat. Commun.*, 2017, **8**, 16098.
36. Y. S. Ding, T. Han, Y. Q. Zhai, D. Reta, N. F. Chilton, R. E. P. Winpenny and Y. Z. Zheng, A Study of Magnetic Relaxation in Dysprosium(III) Single-Molecule Magnets, *Chemistry – A European Journal*, 2020, **26**, 5893-5902.
37. Y.-S. Ding, N. F. Chilton, R. E. P. Winpenny and Y.-Z. Zheng, On Approaching the Limit of Molecular Magnetic Anisotropy: A Near-Perfect Pentagonal Bipyramidal Dysprosium(III) Single-Molecule Magnet, *Angew. Chem. Inter. Ed.*, 2016, **55**, 16071-16074.
38. L. R. Thomas-Hargreaves, M. J. Giansiracusa, M. Gregson, E. Zanda, F. O'Donnell, A. J. Woole, N. F. Chilton and S. T. Liddle, Correlating axial and equatorial ligand field effects to the single-molecule magnet performances of a family of dysprosium bis-methanediide complexes, *Chem. Sci.*, 2021, **12**, 3911-3920.
39. P. Evans, D. Reta, C. A. P. Goodwin, F. Ortu, N. F. Chilton and D. P. Mills, A double-dysprosocenium single-molecule magnet bound together with neutral ligands, *Chem. Commun.*, 2020, **56**, 5677-5680.
40. S. Gupta, S. Dey, T. Rajeshkumar, G. Rajaraman and R. Murugavel, *ChemRxiv*, 2021, DOI: 10.33774/chemrxiv-2021-h3qk7.
41. S. Corner, G. Gransbury, I. Vitorica-Yrezabal, G. Whitehead, N. Chilton and D. Mills, *ChemRxiv*, 2023, DOI: 10.26434/chemrxiv-2023-9l4wm.
42. H. Kong, J.-Y. Wang, J.-C. Liu, L. Zhang, P.-Y. Liao, Y.-Q. Qi, Z. Liu, S.-G. Wu and M.-L. Tong, Photochromic Dysprosium Single-Molecule Magnet Featuring Reversible Redox Transformation of Polyoxomolybdate Moiety, *Angew. Chem. Int. Ed.*, 2024, e202422557.
43. M. Gregson, N. F. Chilton, A.-M. Ariciu, F. Tuna, I. F. Crowe, W. Lewis, A. J. Blake, D. Collison, E. J. L. McInnes, R. E. P. Winpenny and S. T. Liddle, A monometallic lanthanide bis(methanediide) single molecule magnet with a large energy barrier and complex spin relaxation behaviour, *Chem. Sci.*, 2016, **7**, 155-165.
44. Z. Jiang, L. Sun, Q. Yang, B. Yin, H. Ke, J. Han, Q. Wei, G. Xie and S. Chen, Excess axial electrostatic repulsion as a criterion for pentagonal bipyramidal Dy(III) single-ion magnets with high U_{eff} and TB, *J. Mater. Chem.*, 2018, **6**, 4273-4280.
45. Y. Liu, Y.-C. Chen, J. Liu, W.-B. Chen, G.-Z. Huang, S.-G. Wu, J. Wang, J.-L. Liu and M.-L. Tong, Cyanometallate-Bridged Didysprosium Single-Molecule Magnets Constructed with Single-Ion Magnet Building Block, *Inorg. Chem.*, 2020, **59**, 687-694.
46. J. Liu, Y.-C. Chen, J.-L. Liu, V. Vieru, L. Ungur, J.-H. Jia, L. F. Chibotaru, Y. Lan, W. Wernsdorfer, S. Gao, X.-M. Chen and M.-L. Tong, A Stable Pentagonal Bipyramidal Dy(III) Single-Ion Magnet with a Record Magnetization Reversal Barrier over 1000 K, *J. Am. Chem. Soc.*, 2016, **138**, 5441-5450.

47. S. Demir, M. I. Gonzalez, L. E. Darago, W. J. Evans and J. R. Long, Giant coercivity and high magnetic blocking temperatures for N_2^{3-} radical-bridged dilanthanide complexes upon ligand dissociation, *Nat. Commun.*, 2017, **8**, 2144-2144.
48. W. Cai, J. D. Bocarsly, A. Gomez, R. J. Letona Lee, A. Metta-Magaña, R. Seshadri and L. Echegoyen, High blocking temperatures for DyScS endohedral fullerene single-molecule magnets, *Chem. Sci.*, 2020, **11**, 13129-13136.
49. N. Mavragani, D. Errulat, D. A. Gállico, A. A. Kitos, A. Mansikkämäki and M. Murugesu, Radical-Bridged Ln_4 Metallocene Complexes with Strong Magnetic Coupling and a Large Coercive Field, *Angew. Chem. Inter. Ed.*, 2021, **60**, 24206-24213.
50. M. J. Giansiracusa, S. Al-Badran, A. K. Kostopoulos, G. F. S. Whitehead, D. Collison, F. Tuna, R. E. P. Winpenny and N. F. Chilton, A large barrier single-molecule magnet without magnetic memory, *Dalton Trans.*, 2019, **48**, 10795-10798.
51. S. Bala, G.-Z. Huang, Z.-Y. Ruan, S.-G. Wu, Y. Liu, L.-F. Wang, J.-L. Liu and M.-L. Tong, A square antiprism dysprosium single-ion magnet with an energy barrier over 900 K, *Chem. Commun.*, 2019, **55**, 9939-9942.
52. M. Fondo, J. Corredoira-Vázquez, A. M. García-Deibe, J. Sanmartín-Matalobos, S. Gómez-Coca, E. Ruiz and E. Colacio, Slow magnetic relaxation in dinuclear dysprosium and holmium phenoxide bridged complexes: a Dy₂ single molecule magnet with a high energy barrier, *Inorg. Chem. Front.*, 2021, **8**, 2532-2541.
53. X.-Q. Ji, J. Xiong, R. Sun, F. Ma, H.-L. Sun, Y.-Q. Zhang and S. Gao, Enhancing the magnetic performance of pyrazine-*N*-oxide bridged dysprosium chains through controlled variation of ligand coordination modes, *Dalton Trans.*, 2021, **50**, 7048-7055.
54. H. Wu, M. Li, Z. Xia, V. Montigaud, O. Cador, B. Le Guennic, H. Ke, W. Wang, G. Xie, S. Chen and S. Gao, High temperature quantum tunnelling of magnetization and thousand kelvin anisotropy barrier in a Dy₂ single-molecule magnet, *Chem. Commun.*, 2021, **57**, 371-374.
55. Z. Zhu, C. Zhao, Q. Zhou, S. Liu, X.-L. Li, A. Mansikkämäki and J. Tang, Air-Stable Dy(III)-Macrocycle Enantiomers: From Chiral to Polar Space Group, *CCS Chemistry*, 2022, **4**, 3762-3771.
56. X. L. Ding, Y. Q. Zhai, T. Han, W. P. Chen, Y. S. Ding and Y. Z. Zheng, A LocalD_{4h} Symmetric Dysprosium(III) Single-Molecule Magnet with an Energy Barrier Exceeding 2000 K, *Chem. Eur. J.*, 2021, **27**, 2623-2627.
57. J. Xiong, H.-Y. Ding, Y.-S. Meng, C. Gao, X.-J. Zhang, Z.-S. Meng, Y.-Q. Zhang, W. Shi, B.-W. Wang and S. Gao, Hydroxide-bridged five-coordinate Dy(III) single-molecule magnet exhibiting the record thermal relaxation barrier of magnetization among lanthanide-only dimers, *Chem. Sci.*, 2017, **8**, 1288-1294.
58. P. B. Jin, Y. Q. Zhai, K. X. Yu, R. E. P. Winpenny and Y. Z. Zheng, Dysprosiacarboranes as Organometallic Single-Molecule Magnets, *Angew. Chem. Int. Ed.*, 2020, **59**, 9350-9354.
59. A. B. Canaj, S. Dey, O. Céspedes, C. Wilson, G. Rajaraman and M. Murrie, There is nothing wrong with being soft: using sulfur ligands to increase axiality in a Dy(iii) single-ion magnet, *Chem. Commun.*, 2020, **56**, 1533-1536.
60. K. L. M. Harriman, J. Murillo, E. A. Suturina, S. Fortier and M. Murugesu, Relaxation dynamics in see-saw shaped Dy(iii) single-molecule magnets, *Inorg. Chem. Frontiers*, 2020, **7**, 4805-4812.
61. S. Demir, M. D. Boshart, J. F. Corbey, D. H. Woen, M. I. Gonzalez, J. W. Ziller, K. R. Meihaus, J. R. Long and W. J. Evans, Slow Magnetic Relaxation in a Dysprosium Ammonia Metallocene Complex, *Inorg. Chem.*, 2017, **56**, 15049-15056.
62. M. Li, H. Wu, Z. Xia, L. Ungur, D. Liu, L. F. Chibotaru, H. Ke, S. Chen and S. Gao, An Inconspicuous Six-Coordinate Neutral Dy^{III} Single-Ion Magnet with Remarkable Magnetic Anisotropy and Stability, *Inorg. Chem.*, 2020, **59**, 7158-7166.
63. J. Long, I. V. Basalov, N. V. Forosenko, K. A. Lyssenko, E. Mamontova, A. V. Cherkasov, M. Damjanović, L. F. Chibotaru, Y. Guari, J. Larionova and A. A. Trifonov, Dysprosium Single-

- Molecule Magnets with Bulky Schiff Base Ligands: Modification of the Slow Relaxation of the Magnetization by Substituent Change, *Chem. Eur. J.*, 2018, **25**, 474-478.
64. H.-M. Dong, H.-Y. Li, Y.-Q. Zhang, E.-C. Yang and X.-J. Zhao, Magnetic Relaxation Dynamics of a Centrosymmetric Dy₂ Single-Molecule Magnet Triggered by Magnetic-Site Dilution and External Magnetic Field, *Inorg. Chem.*, 2017, **56**, 5611-5622.
 65. T. Han, W. Shi, Z. Niu, B. Na and P. Cheng, Magnetic Blocking from Exchange Interactions: Slow Relaxation of the Magnetization and Hysteresis Loop Observed in a Dysprosium-Nitronyl Nitroxide Chain Compound with an Antiferromagnetic Ground State, *Chem. Eur. J.*, 2012, **19**, 994-1001.
 66. G. Lu, Y. Liu, W. Deng, G.-Z. Huang, Y.-C. Chen, J.-L. Liu, Z.-P. Ni, M. Giansiracusa, N. F. Chilton and M.-L. Tong, A perfect triangular dysprosium single-molecule magnet with virtually antiparallel Ising-like anisotropy, *Inorg. Chem. Front.*, 2020, **7**, 2941-2948.
 67. S. Demir, J. M. Zdrozny and J. R. Long, Large Spin-Relaxation Barriers for the Low-Symmetry Organolanthanide Complexes [Cp*₂Ln(BPh₄)] (Cp* = pentamethylcyclopentadienyl; Ln=Tb, Dy), *Chem. Eur. J.*, 2014, **20**, 9524-9529.
 68. Z. H. Li, Y. Q. Zhai, W. P. Chen, Y. S. Ding and Y. Z. Zheng, Air-Stable Hexagonal Bipyramidal Dysprosium(III) Single-Ion Magnets with Nearly Perfect D_{6h} Local Symmetry, *Chem. Eur. J.*, 2019, **25**, 16219-16224.
 69. S. Jia, X. Zhu, B. Yin, Y. Dong, A. Sun and D.-f. Li, Macroyclic Hexagonal Bipyramidal Dy(III)-Based Single-Molecule Magnets with a D_{6h} Symmetry, *Cryst. Growth Des.* 2023, **23**, 6967-6973.
 70. S.-S. Liu, Y.-S. Meng, Y.-Q. Zhang, Z.-S. Meng, K. Lang, Z.-L. Zhu, C.-F. Shang, B.-W. Wang and S. Gao, A Six-Coordinate Dysprosium Single-Ion Magnet with Trigonal-Prismatic Geometry, *Inorg. Chem.*, 2017, **56**, 7320-7323.
 71. A. G. Bispo-Jr, L. Yeh, D. Errulat, D. A. Gálico, F. A. Sigoli and M. Murugesu, Improving the performance of β-diketonate-based Dy^{III} single-molecule magnets displaying luminescence thermometry, *Chem. Commun.*, 2023, **59**, 8723-8726.
 72. J.-W. Yang, Y.-M. Tian, J. Tao, P. Chen, H.-F. Li, Y.-Q. Zhang, P.-F. Yan and W.-B. Sun, Modulation of the Coordination Environment around the Magnetic Easy Axis Leads to Significant Magnetic Relaxations in a Series of 3d-4f Schiff Complexes, *Inorg. Chem.*, 2018, **57**, 8065-8077.
 73. S. K. Langley, D. P. Wielechowski, V. Vieru, N. F. Chilton, B. Moubaraki, B. F. Abrahams, L. F. Chibotaru and K. S. Murray, A {Cr^{III}₂Dy^{III}₂} Single-Molecule Magnet: Enhancing the Blocking Temperature through 3d Magnetic Exchange, *Angew. Chem. Int. Ed.*, 2013, **52**, 12014-12019.
 74. B.-K. Ling, Y.-Q. Zhai, P.-B. Jin, H.-F. Ding, X.-F. Zhang, Y. Lv, Z. Fu, J. Deng, M. Schulze, W. Wernsdorfer and Y.-Z. Zheng, Suppression of zero-field quantum tunneling of magnetization by a fluorido bridge for a "very hard" 3d-4f single-molecule magnet, *Matter*, 2022, **5**, 3485-3498.
 75. F. Liu, G. Velkos, D. S. Krylov, L. Spree, M. Zalibera, R. Ray, N. A. Samoylova, C.-H. Chen, M. Rosenkranz, S. Schiemenz, F. Ziegs, K. Nenkov, A. Kostanyan, T. Greber, A. U. B. Wolter, M. Richter, B. Büchner, S. M. Avdoshenko and A. A. Popov, Air-stable redox-active nanomagnets with lanthanide spins radical-bridged by a metal–metal bond, *Nat. Commun.*, 2019, **10**, 571.
 76. G. Velkos, D. S. Krylov, K. Kirkpatrick, L. Spree, V. Dubrovin, B. Büchner, S. M. Avdoshenko, V. Bezmelnitsyn, S. Davis, P. Faust, J. Duchamp, H. C. Dorn and A. A. Popov, High Blocking Temperature of Magnetization and Giant Coercivity in the Azafullerene Tb₂@C₇₉N with a Single-Electron Terbium-Terbium Bond, *Angew. Chem. Int. Ed. Engl.*, 2019, **58**, 5891-5896.
 77. J. D. Rinehart, M. Fang, W. J. Evans and J. R. Long, A N₂³⁻ Radical-Bridged Terbium Complex Exhibiting Magnetic Hysteresis at 14 K, *J. Am. Chem. Soc.*, 2011, **133**, 14236-14239.

78. Z. Hu, H. Hu, Z. Chen, D. Liu, Y. Zhang, J. Sun, Y. Liang, D. Yao and F. Liang, Guest-Induced Switching of a Molecule-Based Magnet in a 3d–4f Heterometallic Cluster-Based Chain Structure, *Inorg. Chem.*, 2020, **60**, 633-641.
79. K. R. Meihaus and J. R. Long, Magnetic Blocking at 10 K and a Dipolar-Mediated Avalanche in Salts of the Bis(η^8 -cyclooctatetraenide) Complex $[\text{Er}(\text{COT})_2]^-$, *J. Am. Chem. Soc.*, 2013, **135**, 17952-17957.
80. A. P. Orlova, J. D. Hilgar, M. G. Bernbeck, M. Gembicky and J. D. Rinehart, Intuitive Control of Low-Energy Magnetic Excitations via Directed Dipolar Interactions in a Series of Er(III)-Based Complexes, *J. Am. Chem. Soc.*, 2022, **144**, 11316-11325.
81. H. Kwon, K. R. McClain, J. G. C. Kragskow, J. K. Staab, M. Ozerov, K. R. Meihaus, B. G. Harvey, E. S. Choi, N. F. Chilton and J. R. Long, Coercive Fields Exceeding 30 T in the Mixed-Valence Single-Molecule Magnet $(\text{Cp}i\text{Pr}_5)_2\text{Ho}_2\text{I}_3$, *J. Am. Chem. Soc.*, 2024, **146**, 18714-18721.
82. J. M. Zdrozny, D. J. Xiao, M. Atanasov, G. J. Long, F. Grandjean, F. Neese and J. R. Long, Magnetic blocking in a linear iron(I) complex, *Nat. Chem.*, 2013, **5**, 577-581.
83. A. W. Cook, J. D. Bocarsly, R. A. Lewis, A. J. Touchton, S. Morochnik and T. W. Hayton, An iron ketimide single-molecule magnet $[\text{Fe}_4(\text{N}=\text{CPh}_2)_6]$ with suppressed through-barrier relaxation, *Chem. Sci.*, 2020, **11**, 4753-4757.
84. M. Heu, S. Yoon, B. J. Suh, D.-Y. Jung, J. W. Suk and Y. J. Kim, Magnetic Relaxation in a Single-Molecule Magnet Mn_{12} -chlorobutylate, *J. Kor. Phys. Soc.*, 2003, **43**, 544-547.
85. S. Verma, A. Verma, A. K. Srivastava, A. Gupta, S. P. Singh and P. Singh, Structural and magnetic properties of Mn_{12} -Stearate nanomagnets, *Mater. Chem. Phys.*, 2016, **177**, 140-146.
86. M. Laskowska, O. Pastukh, P. Konieczny, M. Dulski, M. Zalski and L. Laskowski, Magnetic Behaviour of Mn_{12} -Stearate Single-Molecule Magnets Immobilized on the Surface of 300 nm Spherical Silica Nanoparticles, *Materials*, 2020, **13**, 2624.
87. A. Verma, S. Verma, P. Singh and A. Gupta, Ageing effects on the magnetic properties of Mn_{12} -based Acetate and Stearate SMMs, *J. Magn. Magn. Mater.*, 2017, **439**, 76-81.
88. L. A. Kushch, V. D. Sasnovskaya, A. I. Dmitriev, E. B. Yagubskii, O. V. Koplak, L. V. Zorina and D. W. Boukhvalov, New single-molecule magnet based on Mn_{12} oxocarboxylate clusters with mixed carboxylate ligands, $[\text{Mn}_{12}\text{O}_{12}(\text{CN}-\text{o-C}_6\text{H}_4\text{CO}_2)_{12}(\text{CH}_3\text{CO}_2)_4(\text{H}_2\text{O})_4]\cdot 8\text{CH}_2\text{Cl}_2$: Synthesis, crystal and electronic structure, magnetic properties, *Dalton Transactions*, 2012, **41**, 13747-13754.
89. D. Wu, D. Guo, Y. Song, W. Huang, C. Duan, Q. Meng and O. Sato, Co^{II} Molecular Square with Single-Molecule Magnet Properties, *Inorg. Chem.*, 2009, **48**, 854-860.
90. S. K. Gupta, H. H. Nielsen, A. M. Thiel, E. A. Klahn, E. Feng, H. B. Cao, T. C. Hansen, E. Lelièvre-Berna, A. Gukasov, I. Kibalin, S. Dechert, S. Demeshko, J. Overgaard and F. Meyer, Multi-Technique Experimental Benchmarking of the Local Magnetic Anisotropy of a Cobalt(II) Single-Ion Magnet, *JACS Au*, 2023, **3**, 429-440.
91. K. Qian, X.-C. Huang, C. Zhou, X.-Z. You, X.-Y. Wang and K. R. Dunbar, A Single-Molecule Magnet Based on Heptacyanomolybdate with the Highest Energy Barrier for a Cyanide Compound, *J. Am. Chem. Soc.*, 2013, **135**, 13302-13305.